



# Quantum-mimetic imaging

DHEERA VENKATRAMAN  
29 JANUARY 2015 | THESIS DEFENSE



Massachusetts  
Institute of  
Technology

# Outline

1. **Overview:** Quantum metrology and quantum-mimetic imaging
2. **Experiment:** PC-OCT
3. **Experiment:** Classical phase-sensitive ghost imaging
4. **Experiment:** First-photon imaging
5. **Conclusions**

# 1 OVERVIEW

Quantum metrology and quantum-mimetic imaging

# What is quantum metrology?

Experiments that use quantum states of light (e.g. entangled states)

Experiments that use quantum detection methods (e.g. HOM dip)

Cannot be explained by semiclassical theory

# Example: Q-OCT

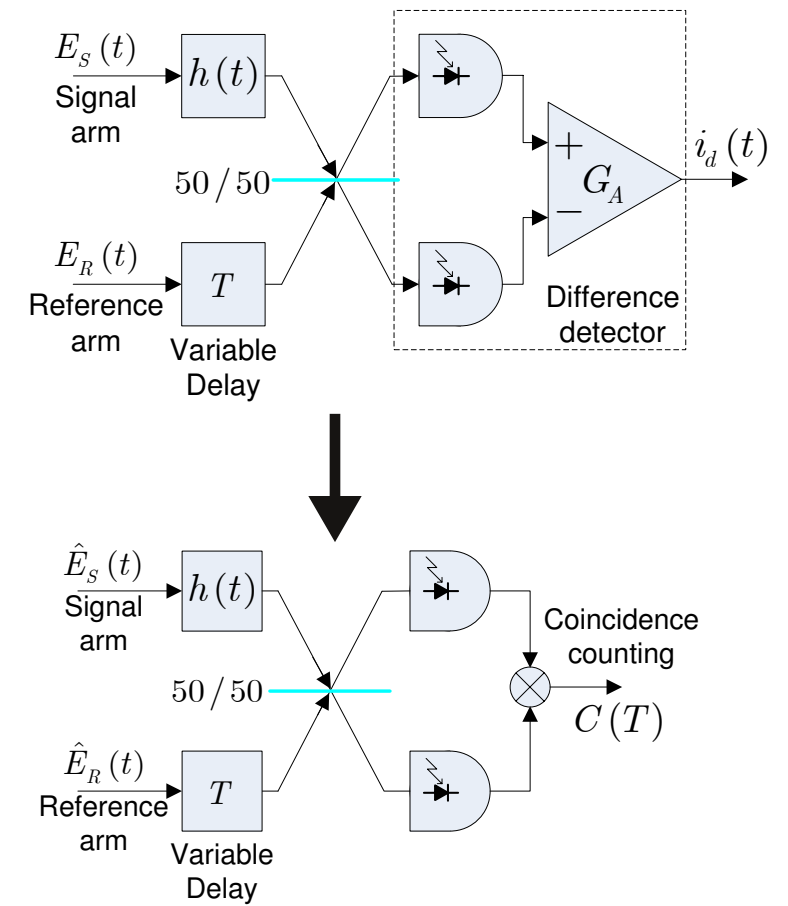
## Quantum optical coherence tomography

Uses an entangled biphoton source

## Advantages

Factor-of-2 resolution improvement  
and even-order dispersion cancellation

Advantages initially attributed to quantum  
physics



B. I. Erkmen and J. H. Shapiro. Phys. Rev. A, 74:041601, Oct 2006.

# Example: Ghost imaging

## Ghost imaging

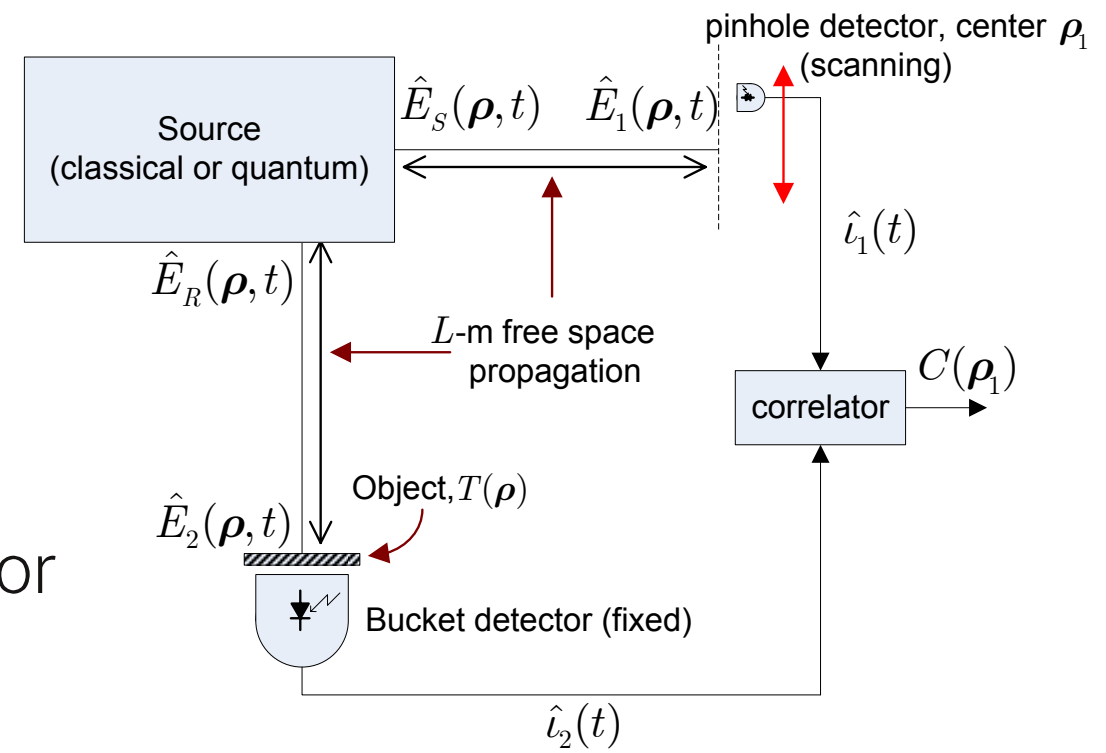
Uses an entangled biphoton source

## Advantages

Images at wavelengths without CCDs

Signal arm only requires a single detector

Initially thought to be uniquely quantum



# Quantum-mimetic imaging

**Quantum imaging** experiments are explained by quantum theories, but their claimed advantages may not necessarily be uniquely quantum.

**Quantum-mimetic imaging** experiments use non-traditional, classical setups to achieve results similar to their quantum counterparts.

# 2 EXPERIMENT

Phase-conjugate optical coherence tomography

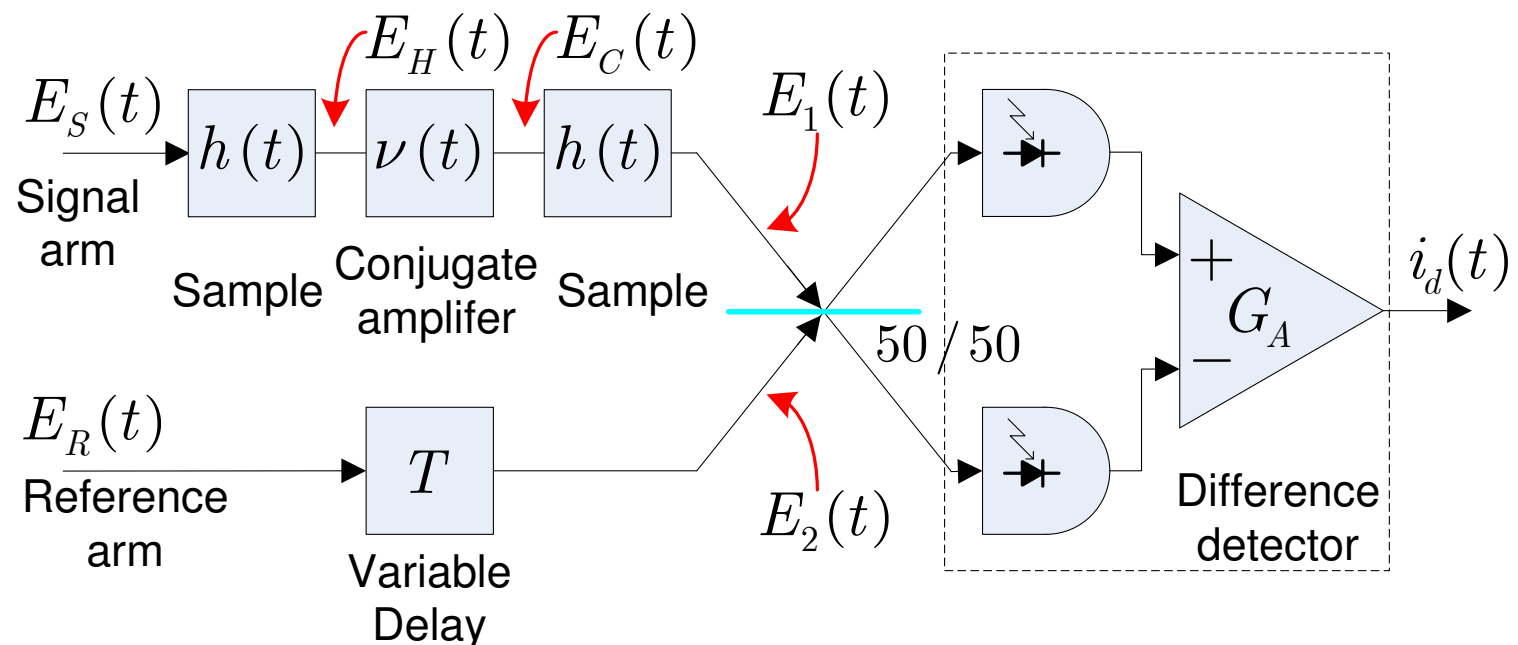
# Motivation

**Q-OCT** advantages (even-order dispersion cancellation, factor-of-2 resolution improvement) shown to originate from phase-sensitive cross-correlations between signal and idler and **not entanglement**

**PC-OCT** employs a classical phase-sensitive source which is **maximally correlated in the classical sens**

# Schematic

**PC-OCT** uses classical phase-sensitive light and a double-pass configuration to obtain similar advantages to Q-OCT



# Comparison of interference signatures

**C-OCT** signature

$$\langle i_d(t) \rangle = 2q\eta G_A \operatorname{Re} \left( \int_{-\infty}^{\infty} \frac{d\Omega}{2\pi} H^*(-\Omega) S(\Omega) e^{-i(\Omega - \omega_0)T} \right)$$

**Q-OCT** signature

$$\langle C(T) \rangle = \frac{q^2 \eta^2}{2} \left[ \int_{-\infty}^{\infty} \frac{d\Omega}{2\pi} |H(\Omega)|^2 S(\Omega) - \operatorname{Re} \left( \int_{-\infty}^{\infty} \frac{d\Omega}{2\pi} H^*(-\Omega) H(\Omega) S(\Omega) e^{-2i\Omega T} \right) \right]$$

**PC-OCT** signature

$$\langle i_d(t) \rangle = 2q\eta G_A \operatorname{Re} \left( \int_{-\infty}^{\infty} \frac{d\Omega}{2\pi} H^*(-\Omega) H(\Omega) \times V^*(-\Omega) S(\Omega) e^{-i(\Omega - \omega_0)T} \right)$$

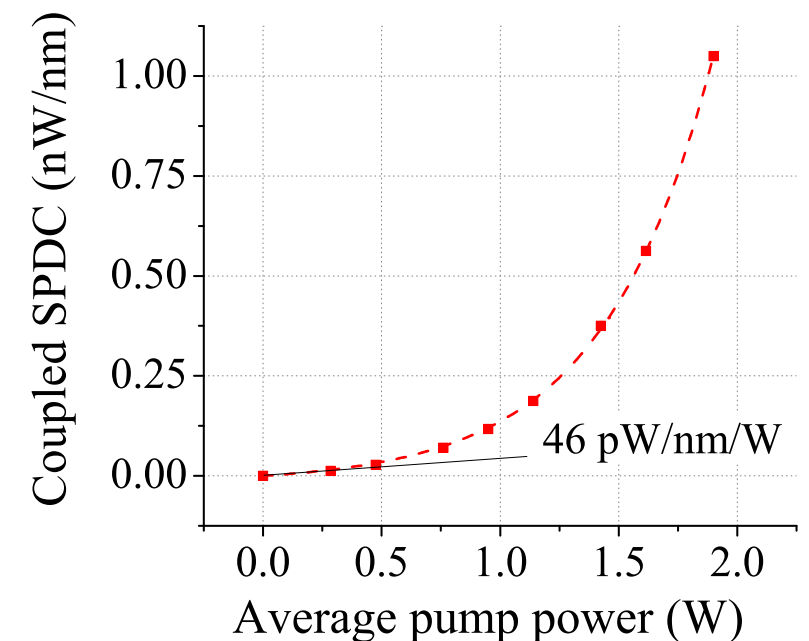
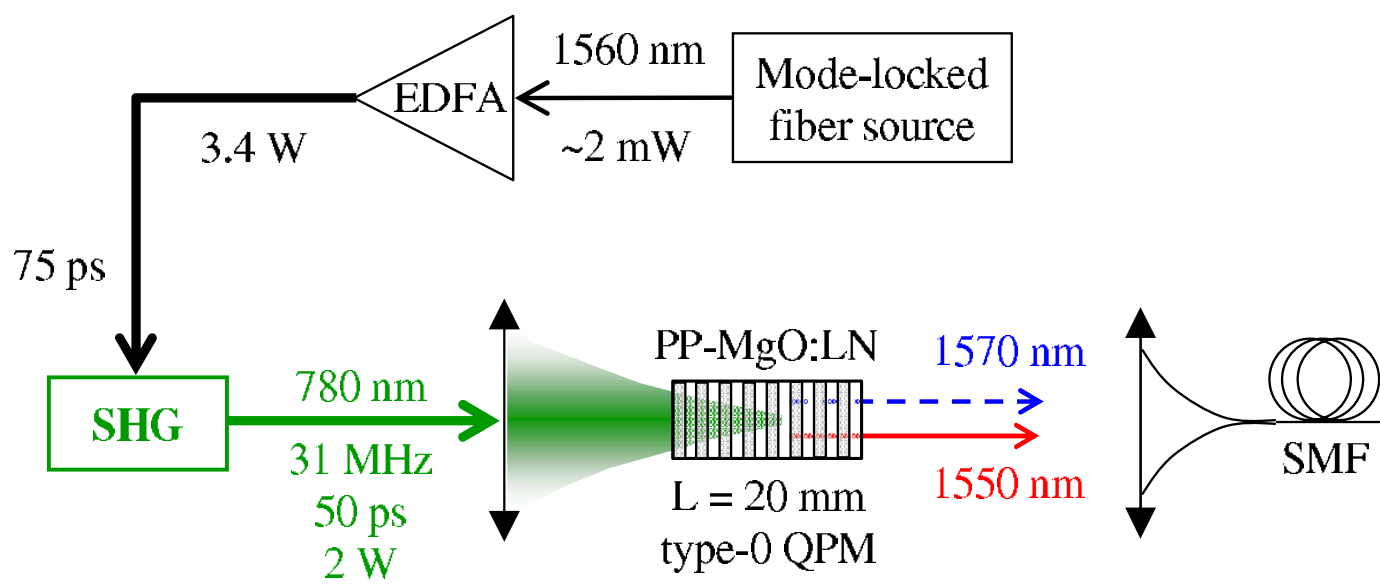


"Quantum-mimetic"

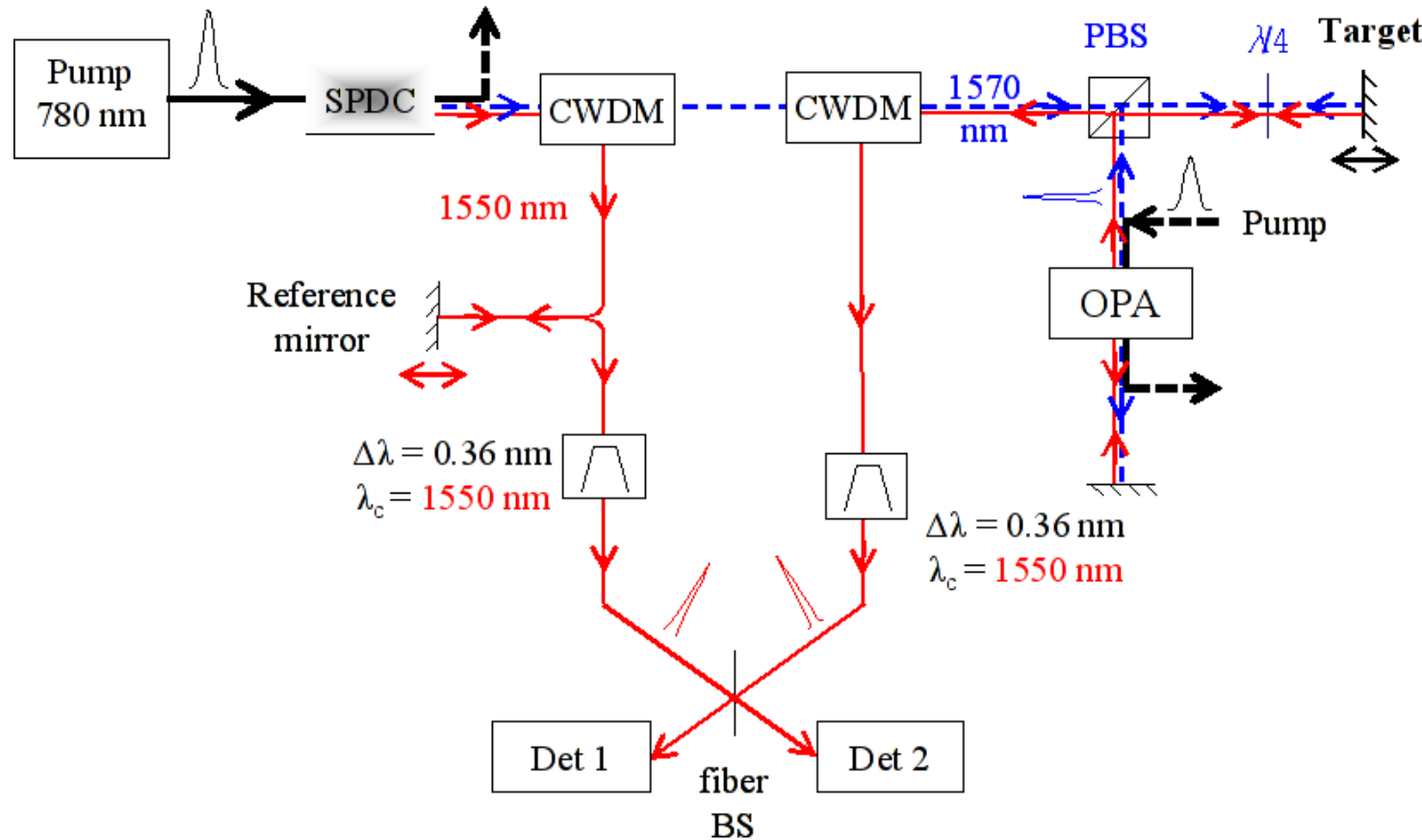
# Classical phase-sensitive light source

Amplified SPDC used to signal and idler beams

Entanglement-breaking; maximally classically correlated



# PC-OCT setup



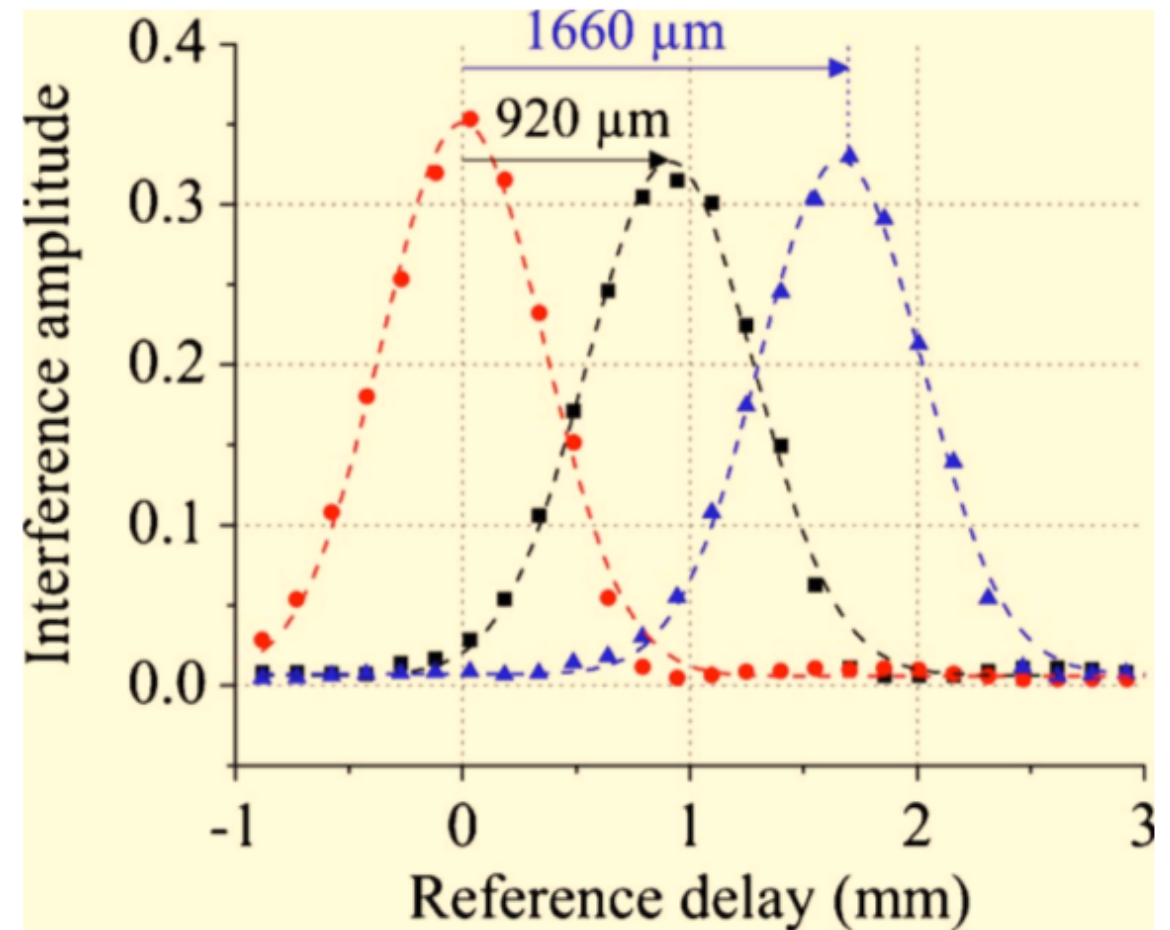
# Results

Translation steps of 450  $\mu\text{m}$

Factor-of-2 resolution improvement visible

Dispersion cancelled almost perfectly

Temperature fluctuations affected long fibers



# 3 EXPERIMENT

Far-field phase-conjugate ghost imaging

# Ghost imaging history

PHYSICAL REVIEW A

VOLUME 52, NUMBER 5

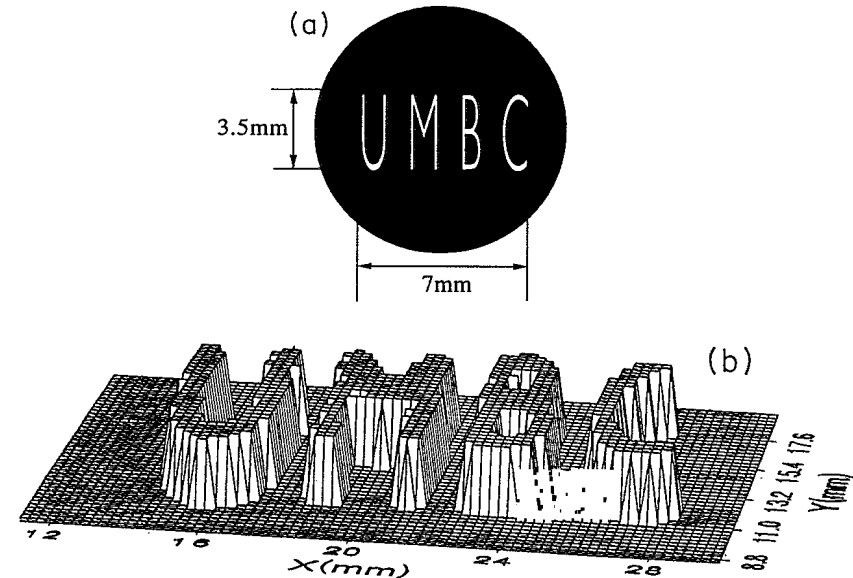
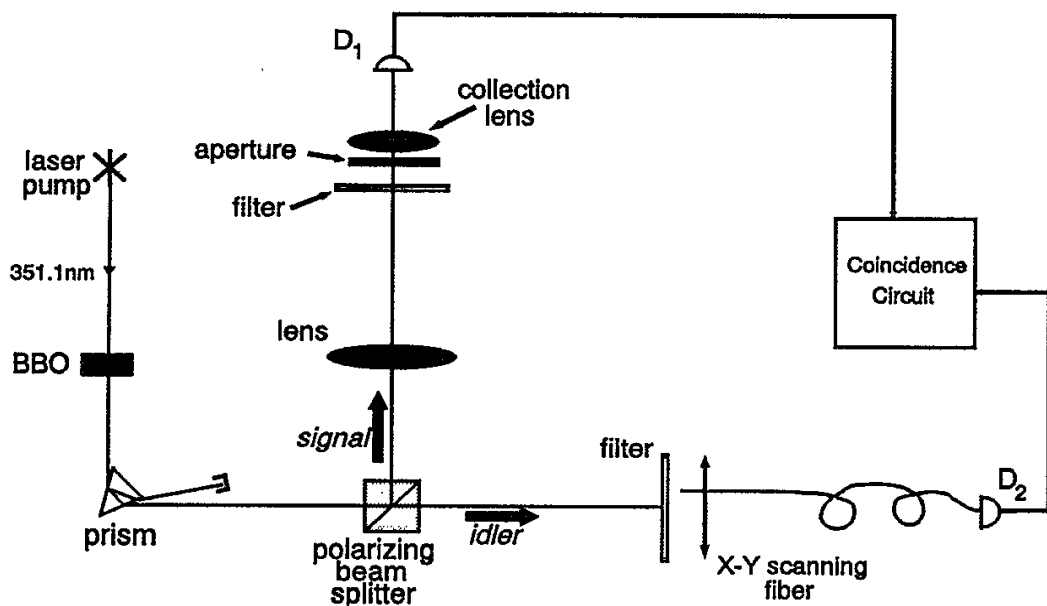
NOVEMBER 1995

## Optical imaging by means of two-photon quantum entanglement

T. B. Pittman, Y. H. Shih, D. V. Strekalov, and A. V. Sergienko

*Department of Physics, University of Maryland Baltimore County, Baltimore, Maryland 21228*

(Received 22 December 1994)



# Ghost imaging history

PRL 94, 063601 (2005)

PHYSICAL REVIEW LETTERS

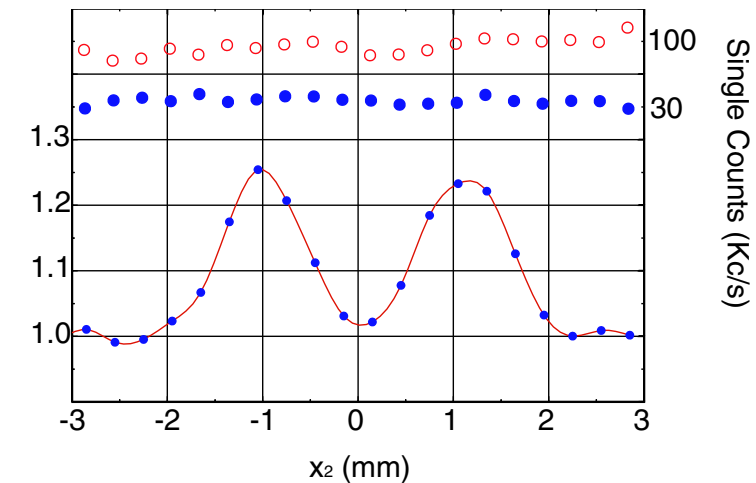
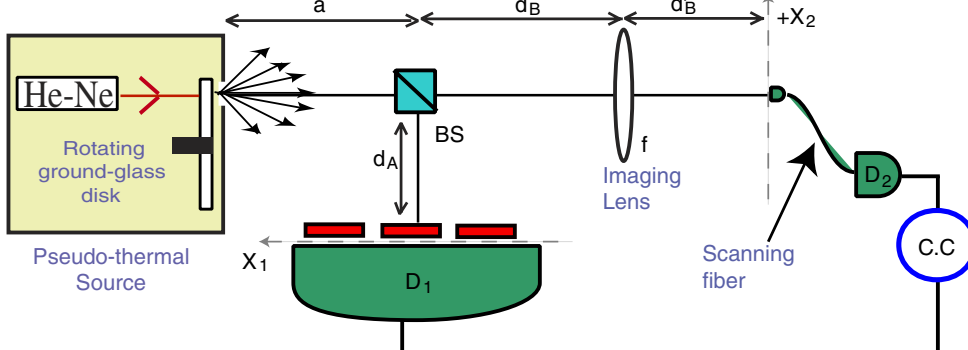
week ending  
18 FEBRUARY 2005

## Two-Photon Imaging with Thermal Light

Alejandra Valencia, Giuliano Scarcelli, Milena D'Angelo, and Yanhua Shih

*Department of Physics, University of Maryland, Baltimore County, Baltimore, Maryland 21250, USA*

(Received 30 July 2004; published 16 February 2005)



# Ghost imaging history

PRL 94, 183602 (2005)

PHYSICAL REVIEW LETTERS

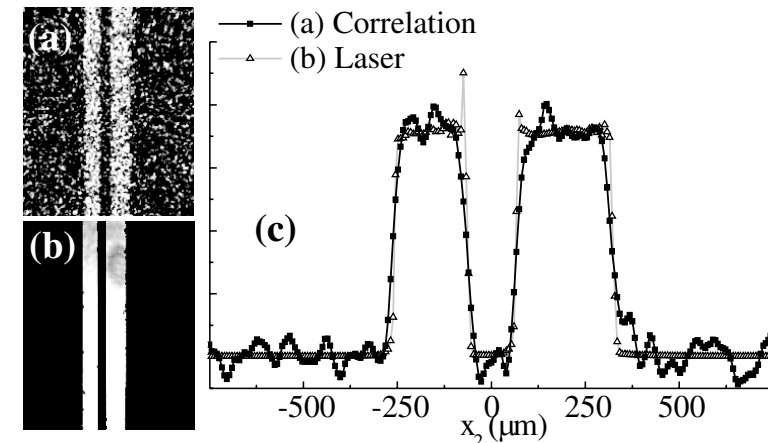
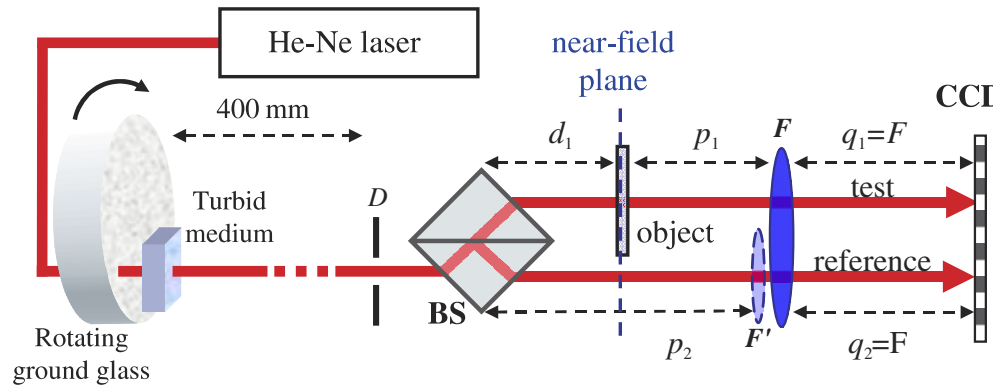
week ending  
13 MAY 2005

## High-Resolution Ghost Image and Ghost Diffraction Experiments with Thermal Light

F. Ferri, D. Magatti, A. Gatti, M. Bache, E. Brambilla, and L. A. Lugiato

INFN, Dipartimento di Fisica e Matematica, Università dell'Insubria, Via Valleggio 11, 22100 Como, Italy

(Received 2 September 2004; published 12 May 2005)



# Ghost imaging history

VOLUME 93, NUMBER 9

PHYSICAL REVIEW LETTERS

week ending  
27 AUGUST 2004

## Ghost Imaging with Thermal Light: Comparing Entanglement and Classical Correlation

A. Gatti, E. Brambilla, M. Bache, and L. A. Lugiato

*INFM, Dipartimento di Fisica e Matematica, Università dell'Insubria, Via Valleggio 11, 22100 Como, Italy*

(Received 25 July 2003; published 26 August 2004)

We consider a scheme for coherent imaging that exploits the classical correlation of two beams obtained by splitting incoherent thermal radiation. This case is analyzed in parallel with the configuration based on two entangled beams produced by parametric down-conversion, and a precise formal analogy is pointed out. This analogy opens the possibility of using classical beams from thermal radiation for ghost imaging schemes in the same way as entangled beams.

DOI: 10.1103/PhysRevLett.93.093602

PACS numbers: 42.50.-p, 42.50.Dv, 42.50.Ar

# Ghost imaging history

## Unified Theory of Ghost Imaging with Gaussian-State Light

Baris I. Erkmen\* and Jeffrey H. Shapiro

*Massachusetts Institute of Technology, Research Laboratory of Electronics, Cambridge, Massachusetts 02139, USA*

(Dated: February 2, 2008)

The theory of ghost imaging is developed in a Gaussian-state framework that both encompasses prior work—on thermal-state and biphoton-state imagers—and provides a complete understanding of the boundary between classical and quantum behavior in such systems. The core of this analysis is the expression derived for the photocurrent-correlation image obtained using a general Gaussian-state source. This image is expressed in terms of the phase-insensitive and phase-sensitive cross-correlations between the two detected fields, plus a background. Because any pair of cross-correlations is obtainable with classical Gaussian states, the image does not carry a quantum signa-

Erkmen and Shapiro showed

1. Ghost imaging is not unique to quantum light sources
2. **Phase-sensitive ghost imaging** can also be implemented classically

# Another classical phase-sensitive source

In PC-OCT, we implemented a classical phase-sensitive light source using **amplified SPDC**

For GI we use **a pair of spatial-light modulators** (SLMs) driven with deterministic, anti-correlated pseudorandom phases



# SLM principles of operation

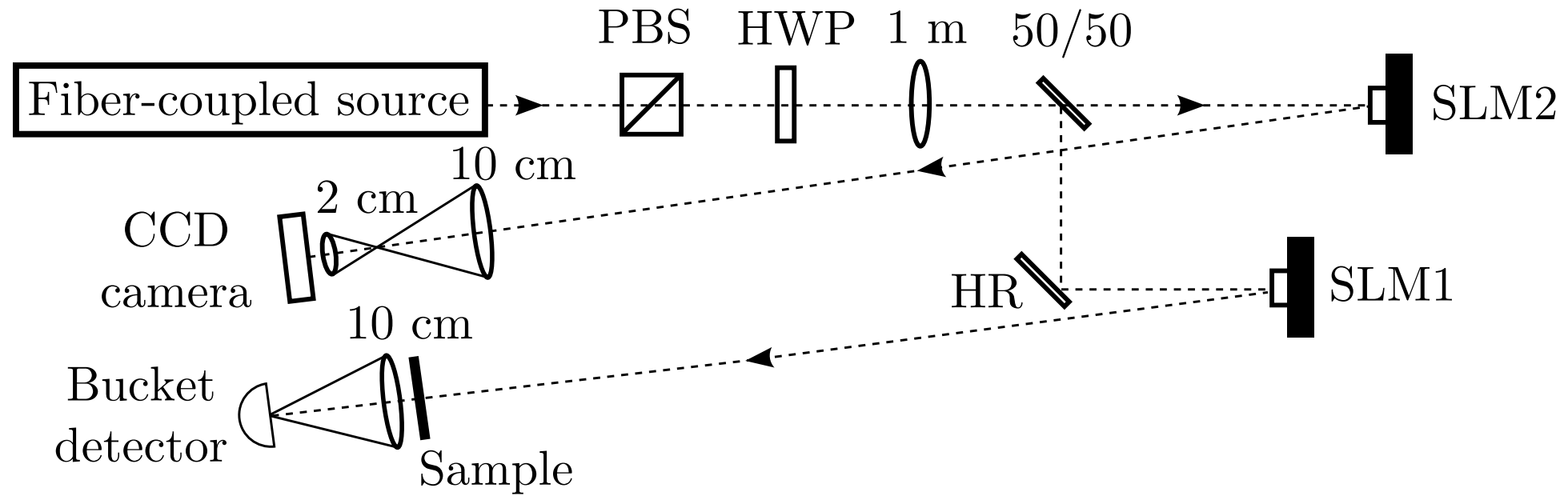
**Mechanically-driven SLMs** translate individual pixels using piezoelectric transducers or MEMS devices and are polarization-independent

- » Pros: high-speed modulation (10-100 kHz)
- » Cons: pixel cross-talk, expensive

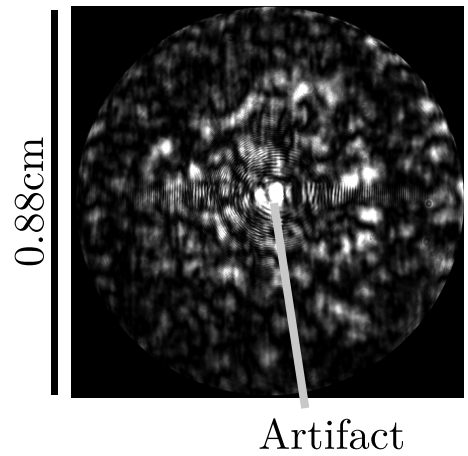
**Liquid-crystal SLMs** use electric field and are polarization-dependent

- » Pros: low cross-talk, convenient to convert to intensity modulator
- » Cons: slow (~1-100 Hz), calibration issues, dead region

# Experimental setup

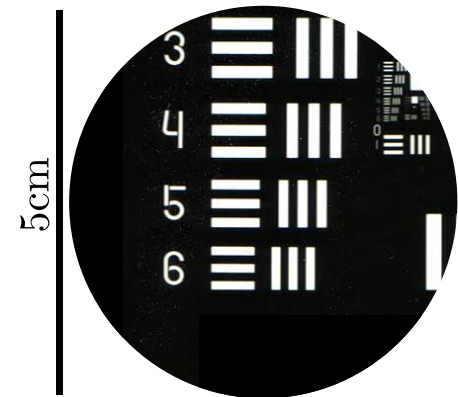


# Results



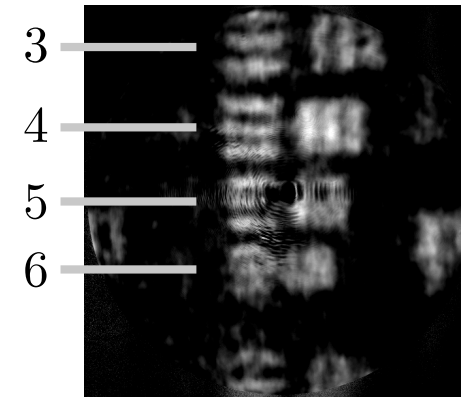
0.88cm

Artifact

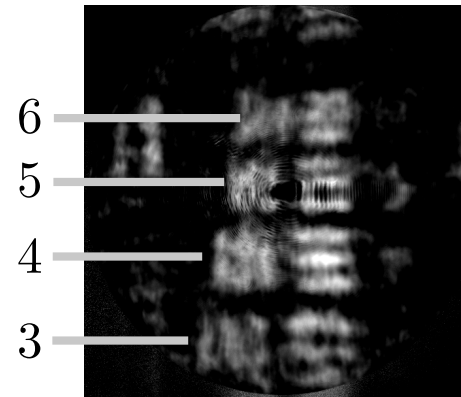


Sample speckle pattern as seen by CCD

USAF resolution test transmission mask

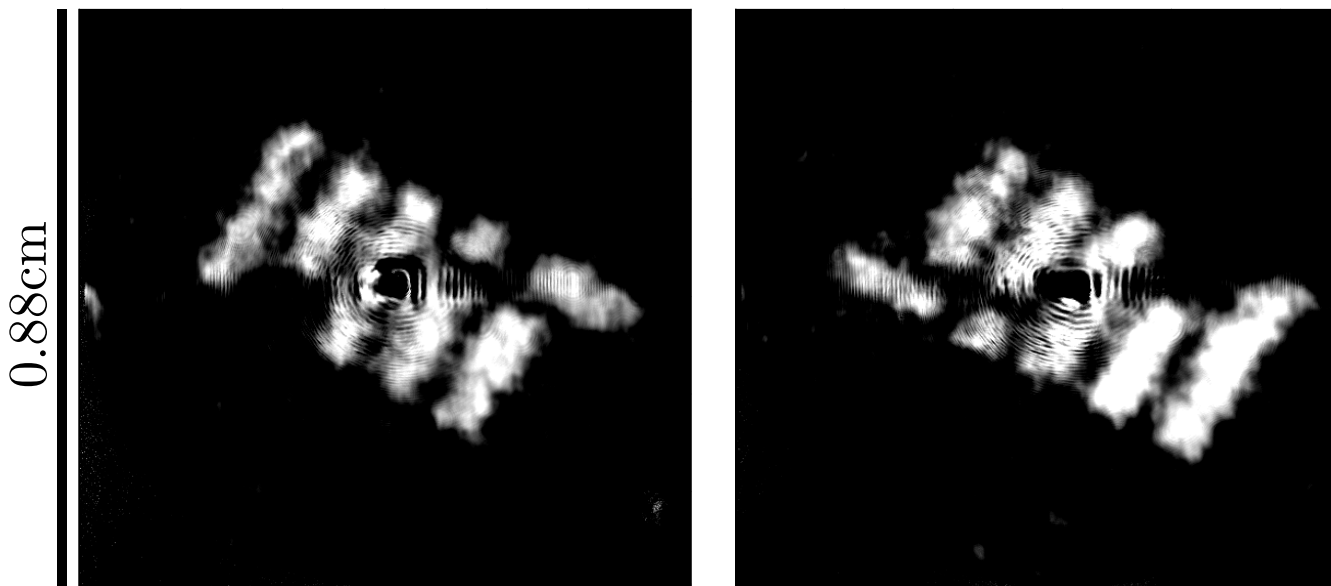


Phase-insensitive ghost imaging result (upright)



Phase-sensitive ghost imaging result (inverted)

# Results

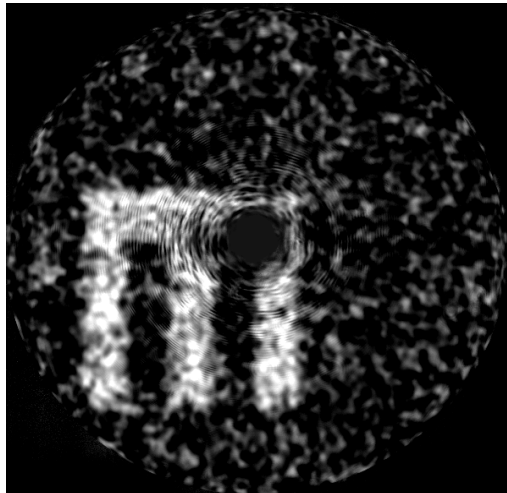


Phase-insensitive

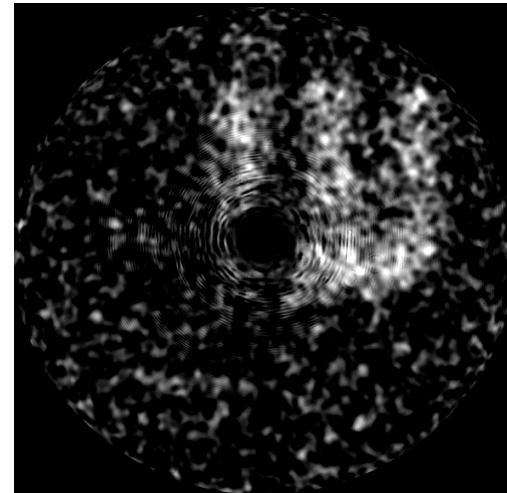
Phase-sensitive

# Results

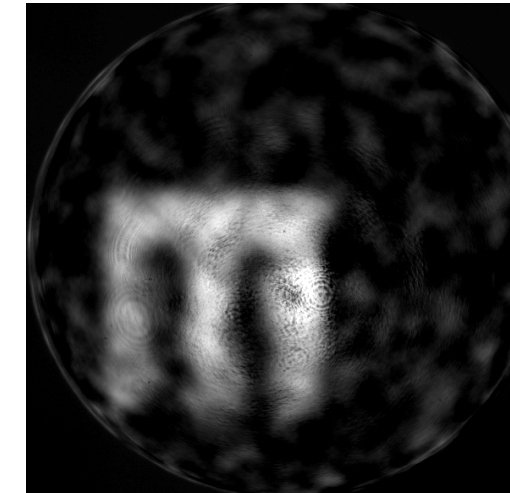
Phase-sensitive operation highly sensitive to focusing parameters if SLMs not located at beam waist ( $2.75 z_R$  in this case)



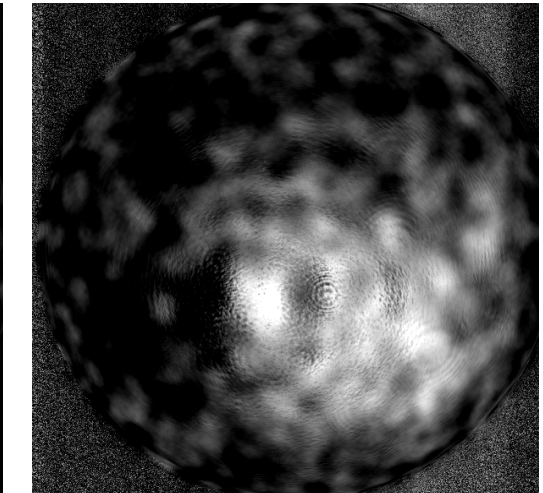
Phase-insensitive



Phase-sensitive



Phase-insensitive



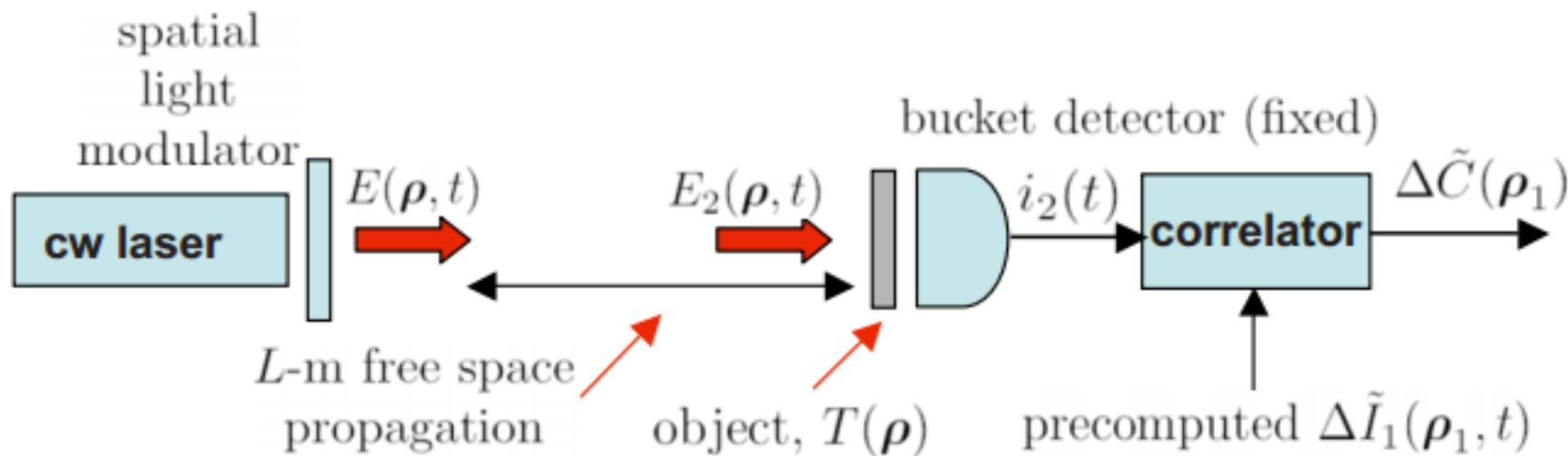
Phase-sensitive

Loose focusing

Tight focusing

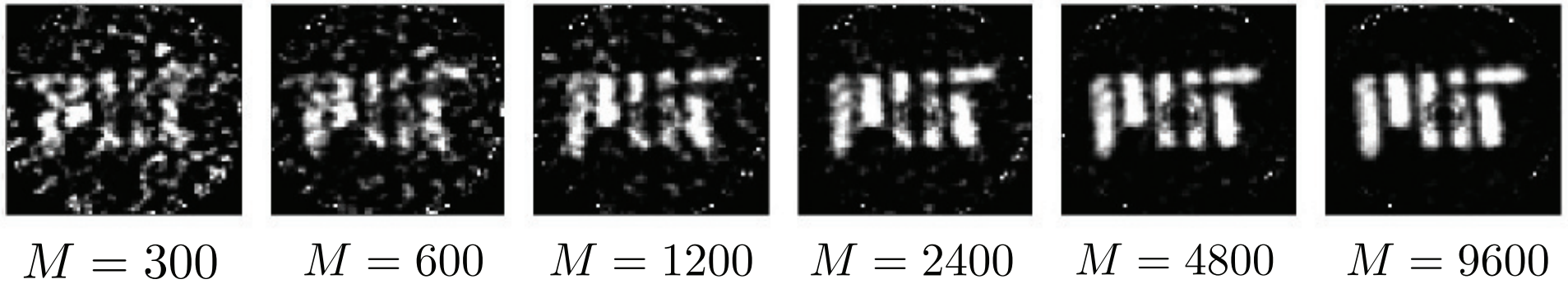
# Computational ghost imaging

Since both signal and reference arm phase patterns are deterministic, we can replace the reference arm with a simulation

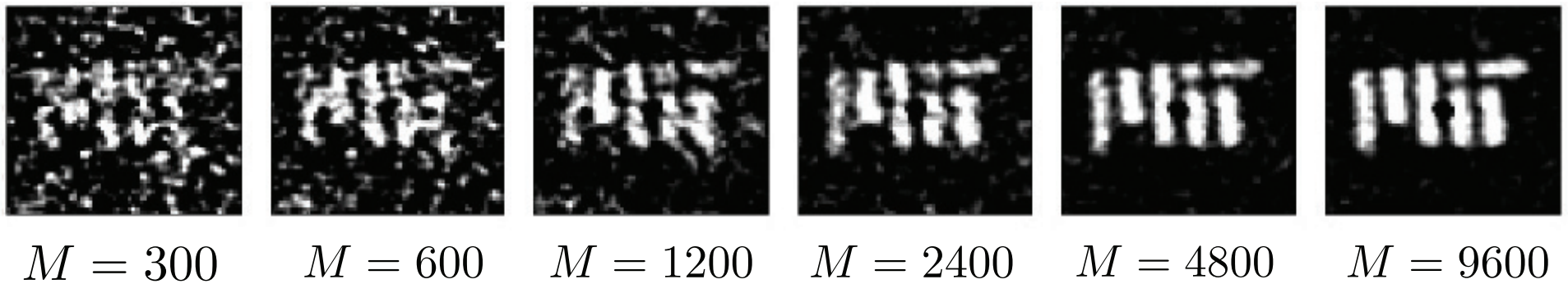


# Computational ghost imaging

Physical



Simulated

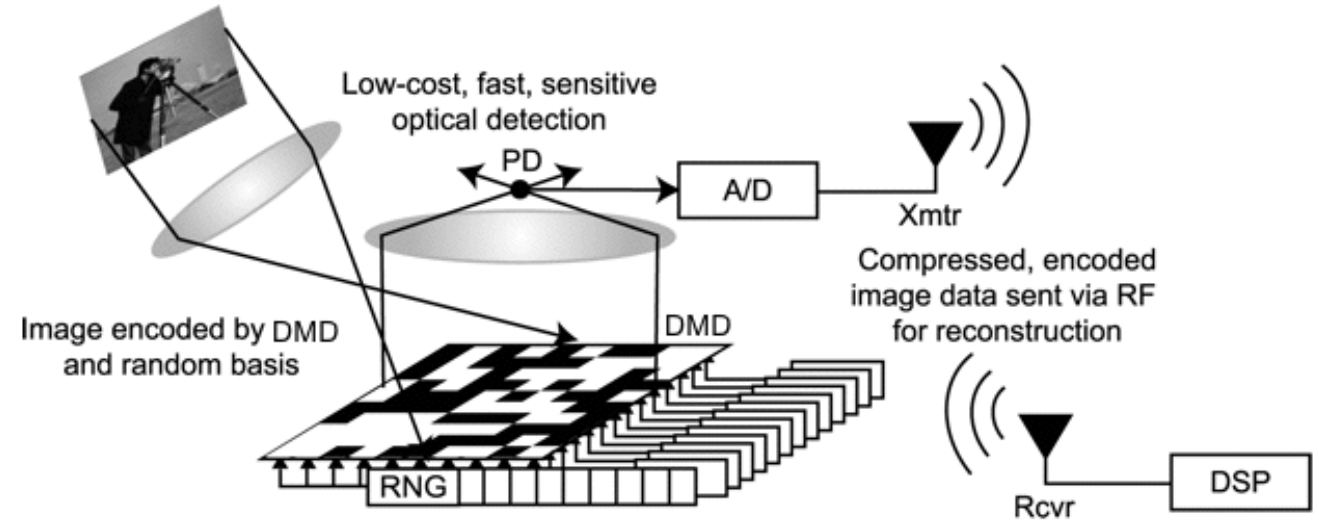


# Compressive ghost imaging

Averaging over several thousand realizations is slow

GI similar to Rice University single-pixel camera

Assume object has spatial structure; use computational optimization to recover object



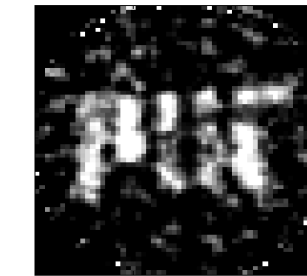
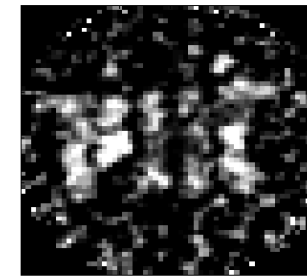
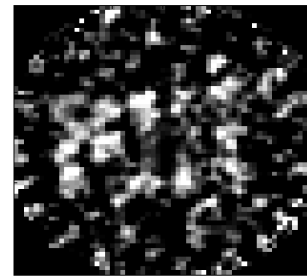
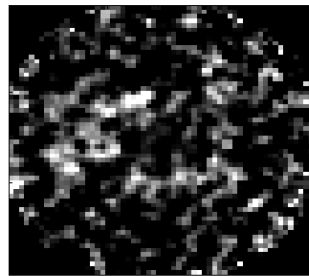
M.F. Duarte, et al. Signal Processing Magazine, IEEE, 25(2):83–91, March 2008.

$$\hat{x} = \arg \min_x \|W\{x\}\|_1, \text{ s. t. } \|Ax - b\|_2 < \epsilon$$

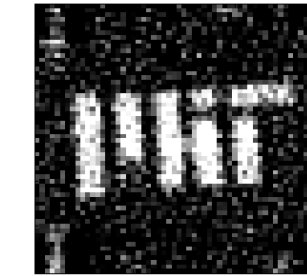
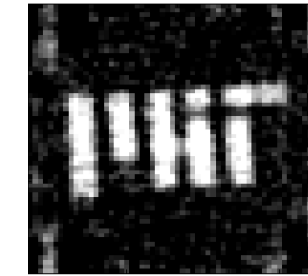
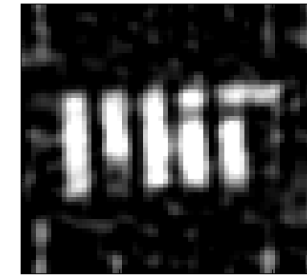
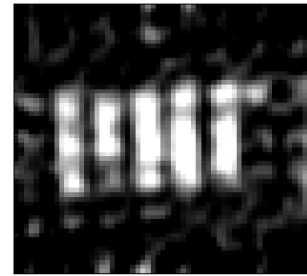
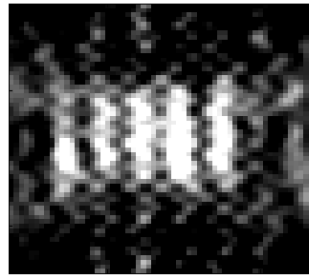
# Compressive ghost imaging

Factor of  $\sim 10$  speedup by using compressive sensing in DCT basis

BS + CCD GI



BS + CCD GI  
(L1 min DCT)



M=100

M=200

M=400

M=800

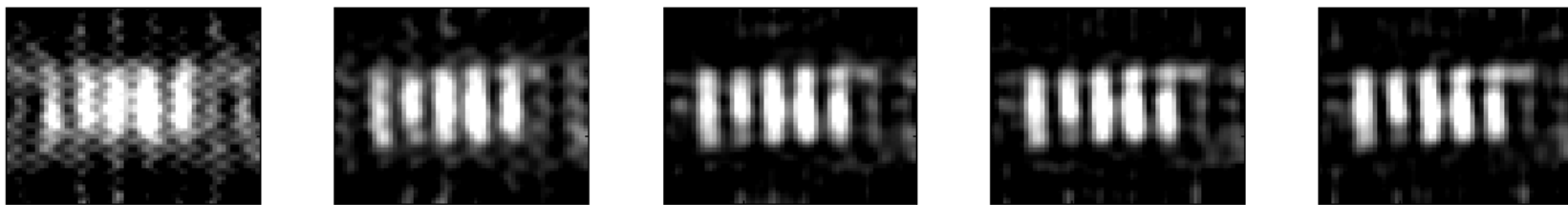
M=1200

M=4800

# Compressive ghost imaging

Total variation instead of DCT gives even faster results for binary masks

(a) DCT



(b) TV



100

200

400

600

800

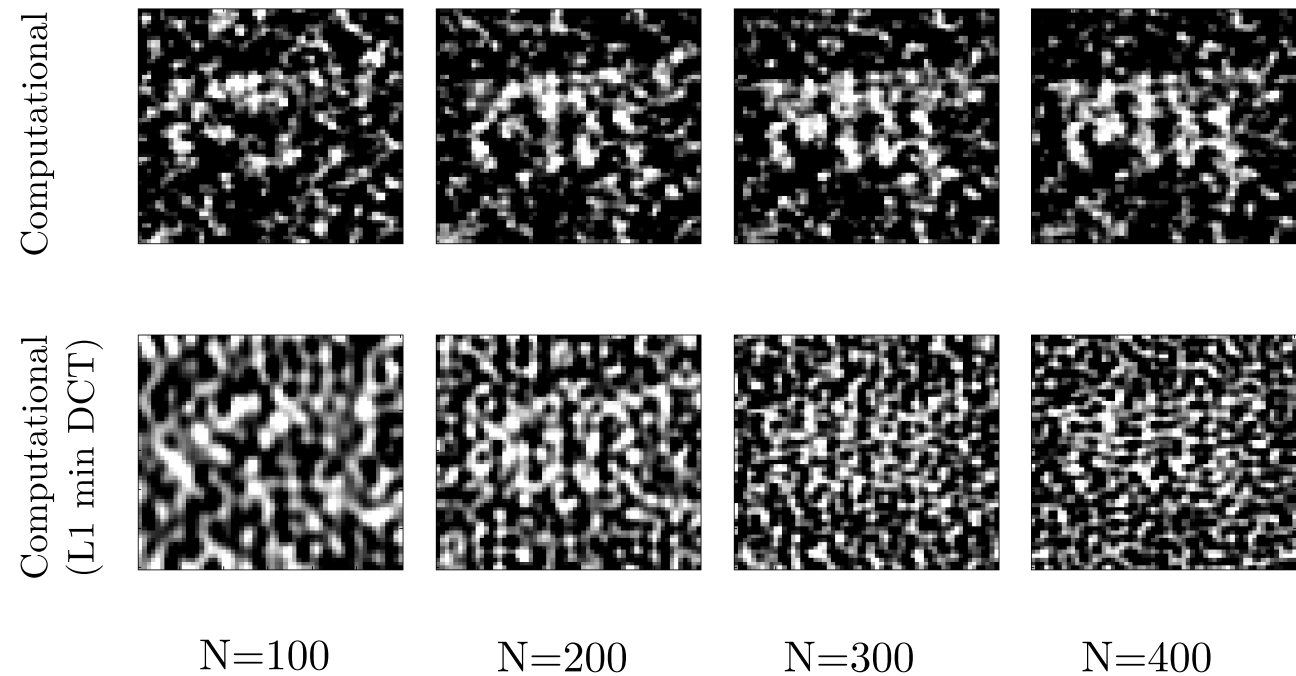
Number of realizations

# Computational compressive GI

Does not work as expected

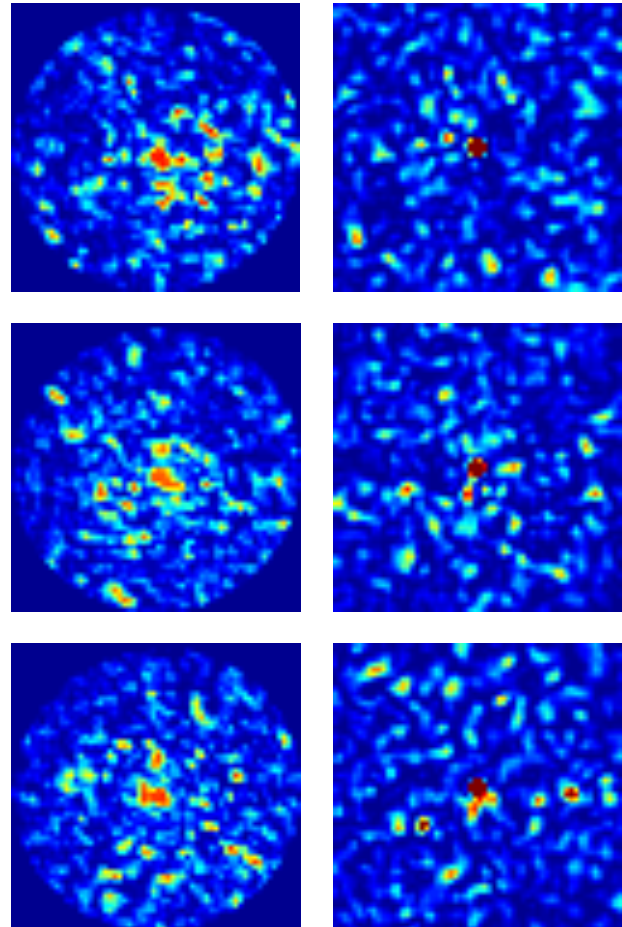
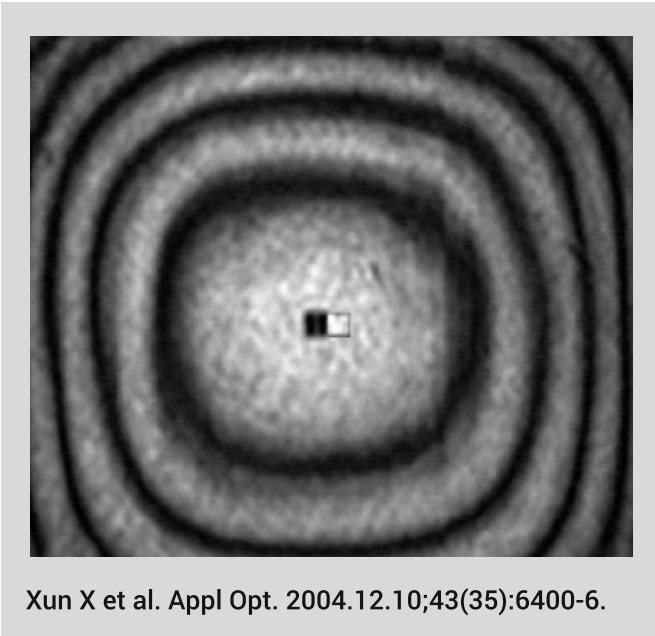
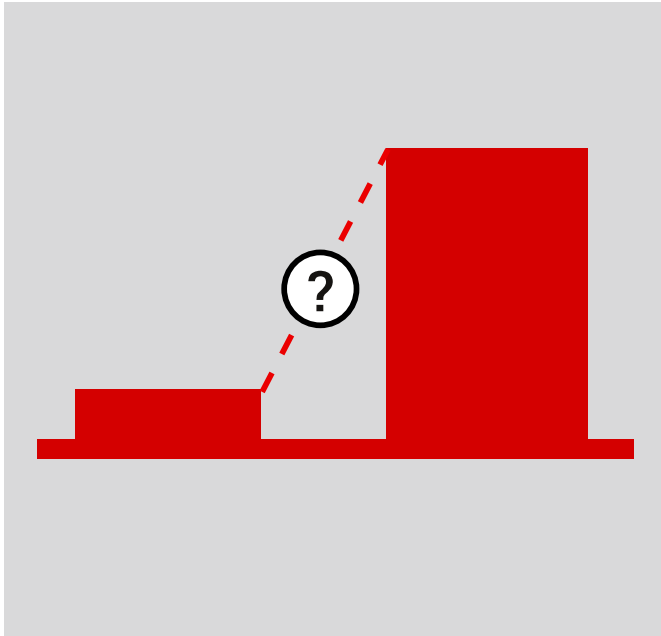
**SLM imperfections:** dead-space behavior, flatness, calibration

In **compressive GI** we used a beamsplitter so did to see effects of these imperfections



In **computational GI** we averaged out the imperfections over thousands of realizations

# SLM imperfections



## Dead-space behavior

May have cross-talk  
with active pixels

## SLM not flat

Several-wavelength  
deviations

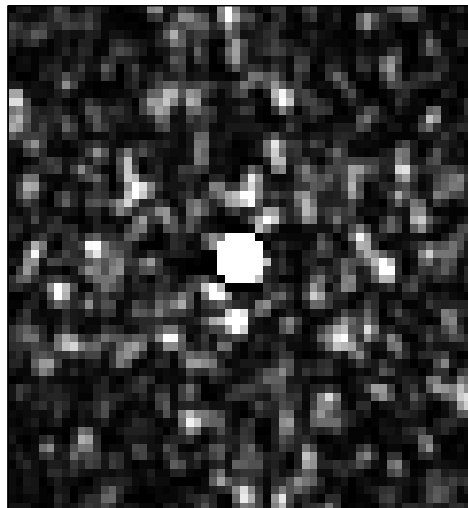
CCD image

Simulation

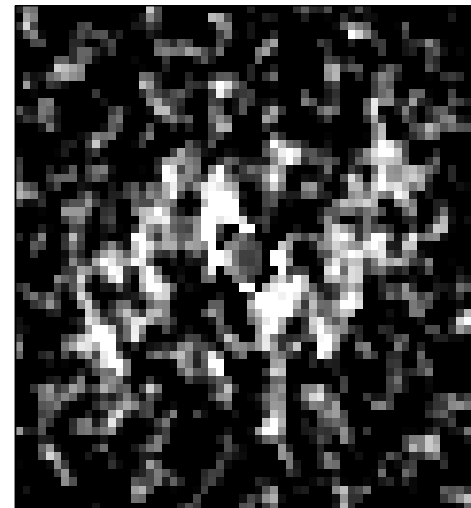
# Computational compressive GI

Need more predictable **SLM** for far-field ghost imaging

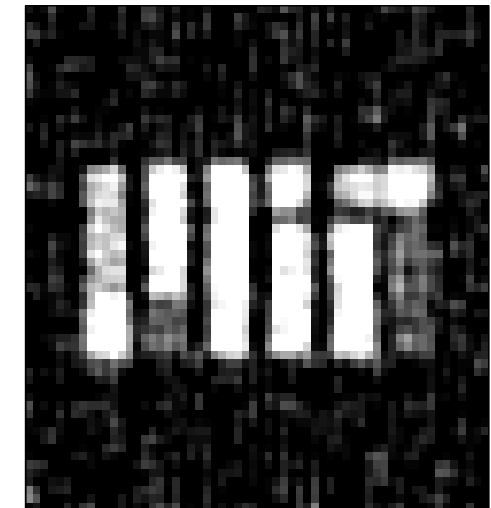
**Digital micromirror devices** more predictable, but since they only modulate reflectivity and not phase, they are only suitable for near-field operation



Sample speckle



Averaging (M=500)



CS (M=500)

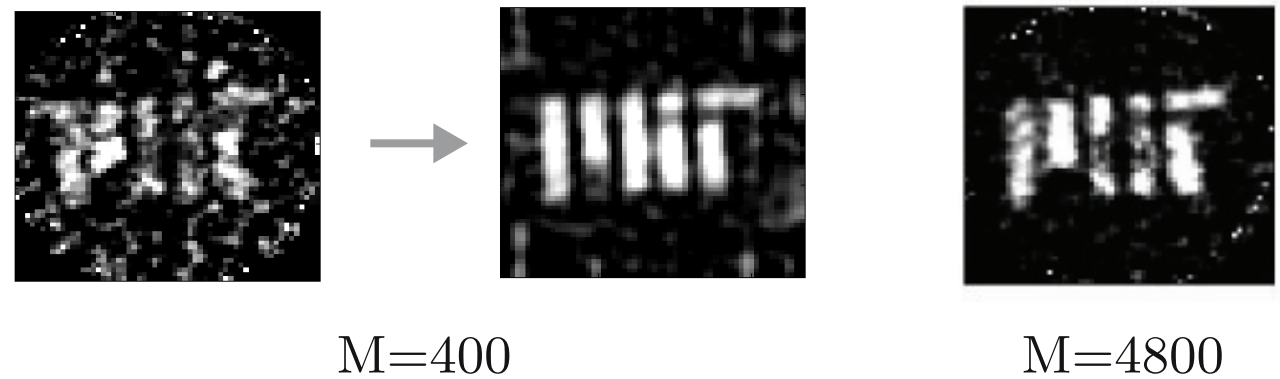
DMD simulation results show phase-sensitive (inverted) and phase-insensitive (upright) images superimposed. CS helps in recovery but not 100%.

# 4 EXPERIMENT

Single-photon imaging

# Motivation

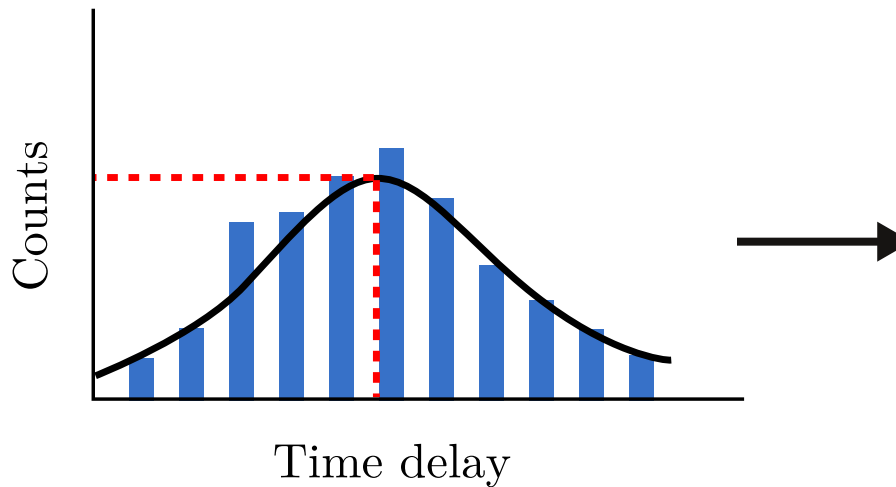
In ghost imaging, we used computational reconstruction to recover a clean image using a small number of measurements



Can we use this for depth and reflectivity imaging in a more general sense?

# Traditional active imaging

Use pulsed, periodic illumination and histogram **tens to hundreds of photons per pixel** of data to obtain accurate depth and reflectivity maps



One-pixel histogram



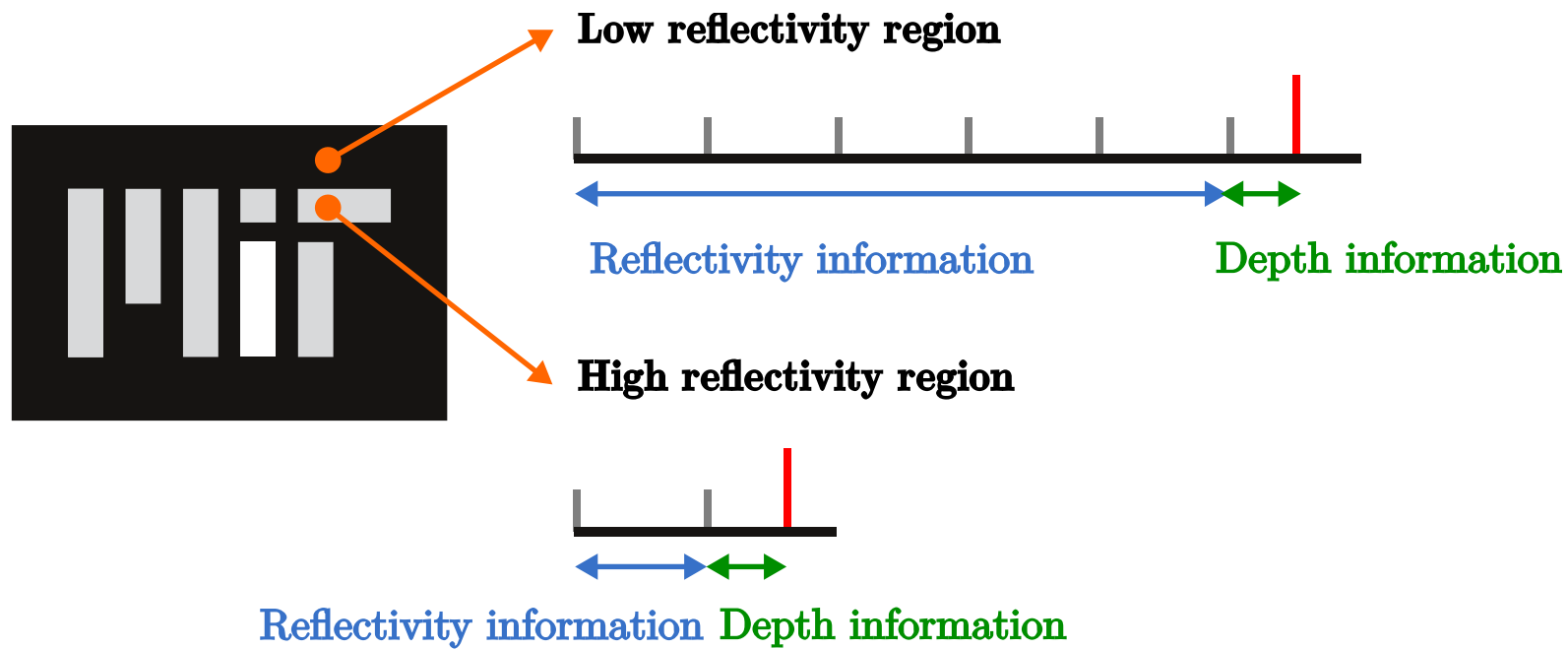
Reflectivity map



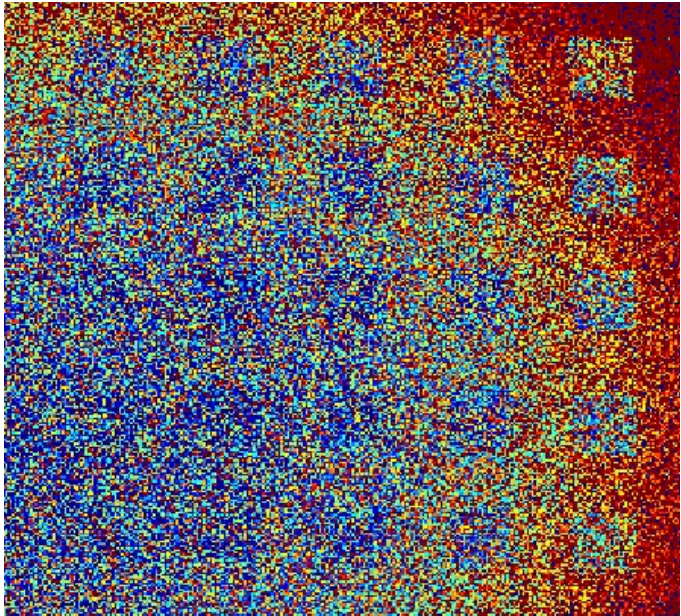
Depth map

# First-photon imaging

What if we only used **1 photon per pixel**?



# First-photon imaging



## Problem:

Poor-quality images, corrupted by pulse width (depth) and Poisson noise (reflectivity)



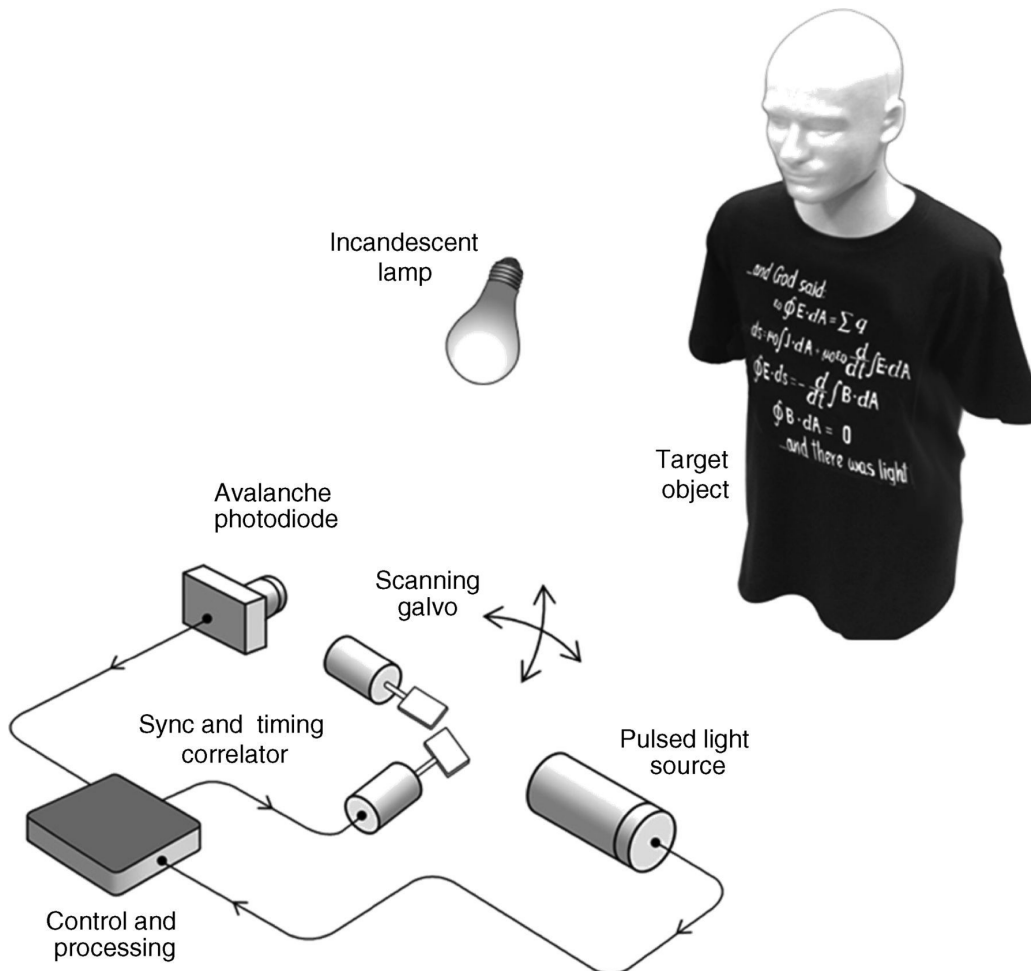
## Solution:

Use knowledge of single-photon detection statistics

Similar to compressive GI, assume object is realistic and has spatial correlations

Use computational optimization to reconstruct the scene given a small amount of data (1 photon per pixel)

# Experimental setup



## Illumination:

Laser: 640-nm, 10 MHz repetition rate,  
226-ps RMS width

## Raster scanning:

2-axis galvo mirror:  $\pm 20^\circ$ , 1000×1000 scan

## Detection:

APD: 100×100  $\mu\text{m}$ , 50-ps jitter, 35% efficiency  
IF: 2-nm bandwidth, 49% transmission  
TDC: 8-ps resolution

# Computational reconstruction algorithm

## Step 1: Reflectivity reconstruction

Minimize a weighted sum of the log-likelihood given Poisson statistics and a sparsity-promoting term:

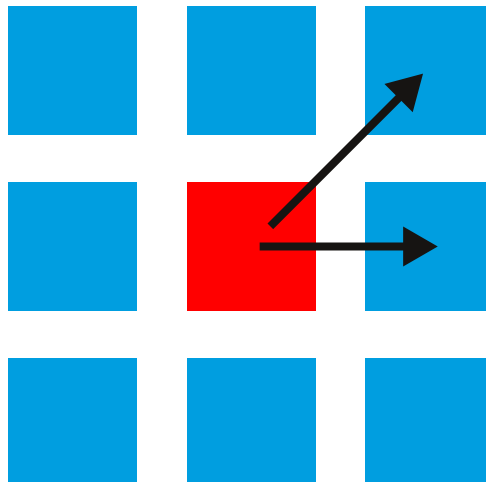
$$\{\hat{\alpha}(x, y)\} = \arg \min_{\{\alpha(x, y)\}} (1 - \beta) \left[ \sum_x \sum_y \mathcal{L}(\alpha(x, y) | n(x, y)) \right] + \beta \|\Phi(\{\alpha(x, y)\})\|_1$$

$$\mathcal{L}(\alpha(x, y) | n(x, y)) = \gamma [\alpha(x, y)S + BT_r] [n(x, y) - 1] - \log [\gamma \alpha(x, y)S + BT_r]$$

# Computational reconstruction algorithm

## Step 2: Background noise censoring

Background noise makes depth reconstruction non-convex. We eliminate background photons using the ROAD statistic:

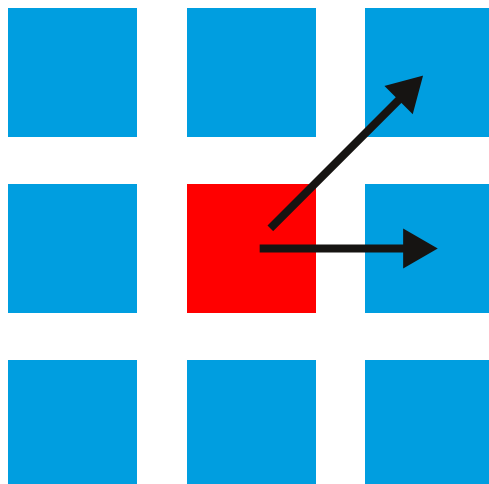


1. Calculate differences to nearest 8 pixels $|t(x_1, y_1) - t(x, y)|, \dots, |t(x_8, y_8) - t(x, y)|$
2. Sort in ascending order
3. Define  $\text{ROAD}(x, y)$  to be the sum of the first 4 values

# Computational reconstruction algorithm

## Step 2: Background noise censoring

Background noise makes depth reconstruction non-convex. We eliminate background photons using the ROAD statistic:



4. Binary decision test: If  $\text{ROAD}(x, y) > C$ , reject pixel and replace with average of neighboring 8 pixels.

$$C = 4T_p \frac{BT_r}{\hat{\alpha}(x, y)S + BT_r}$$

# Computational reconstruction algorithm

## Step 3: Depth reconstruction

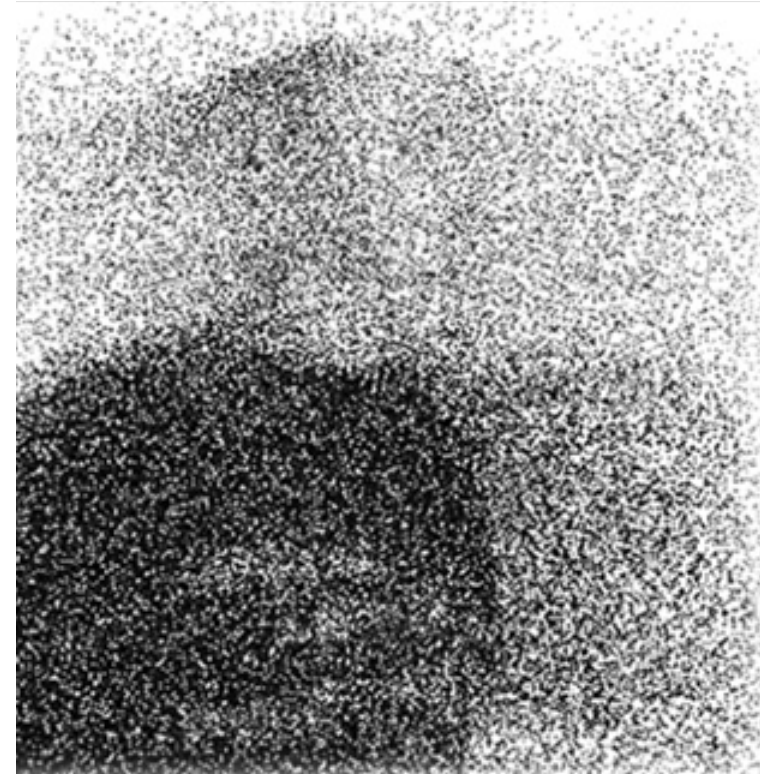
Minimize a weighted sum of the log-likelihood given pulse shape and a sparsity-promoting term:

$$\{\hat{Z}(x, y)\} = \arg \min_{\{Z(x, y)\}} (1 - \beta) \left[ \sum_x \sum_y \mathcal{L}(Z(x, y) | t(x, y)) \right] + \beta \|\Phi(\{Z(x, y)\})\|_1$$

$$\mathcal{L}(Z(x, y) | t(x, y)) = -\log \left[ s(t(x, y) - \frac{2Z(x, y)}{c}) \right]$$

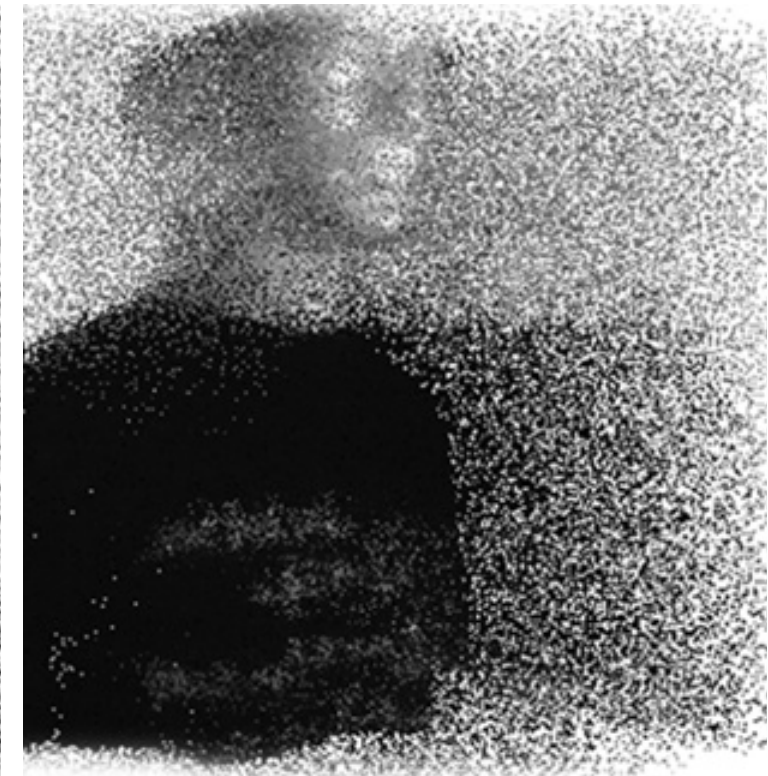
# Results

## Raw ML estimates



# Results

## Reflectivity reconstruction



# Results

## Background noise censoring

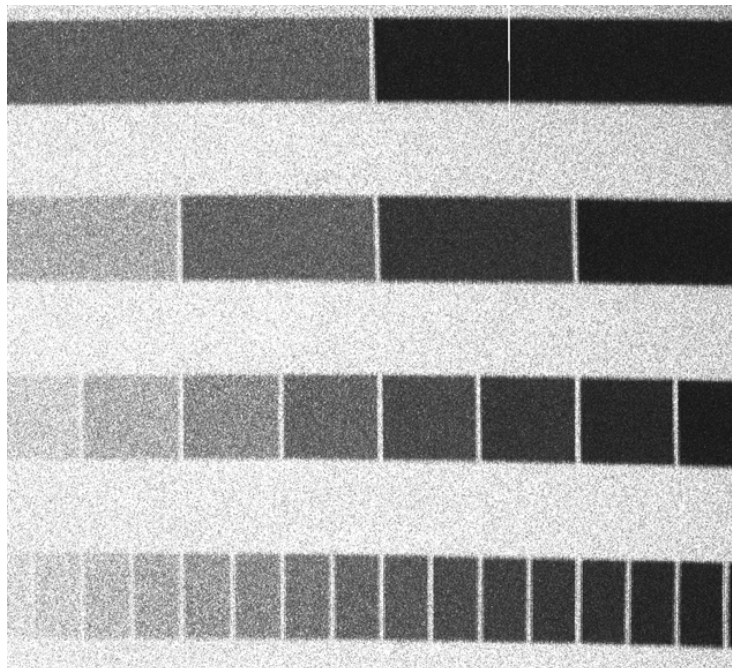


# Results

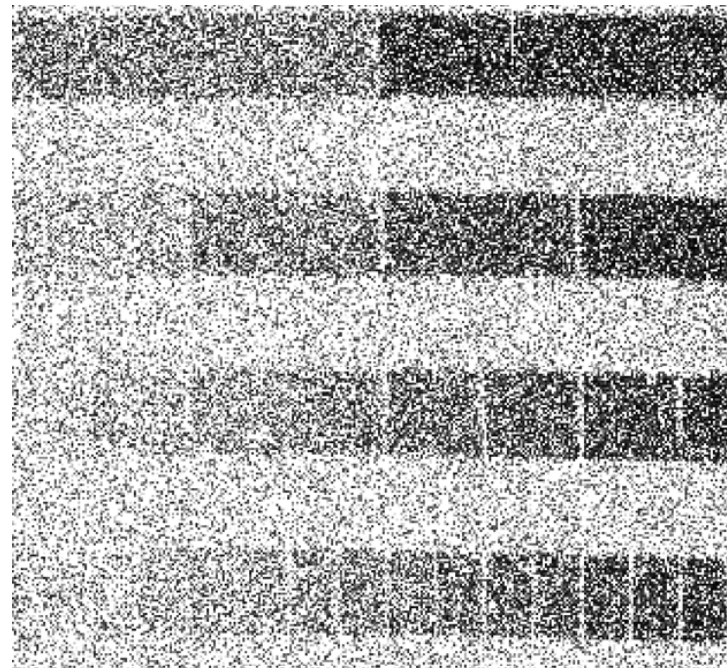
## Depth reconstruction



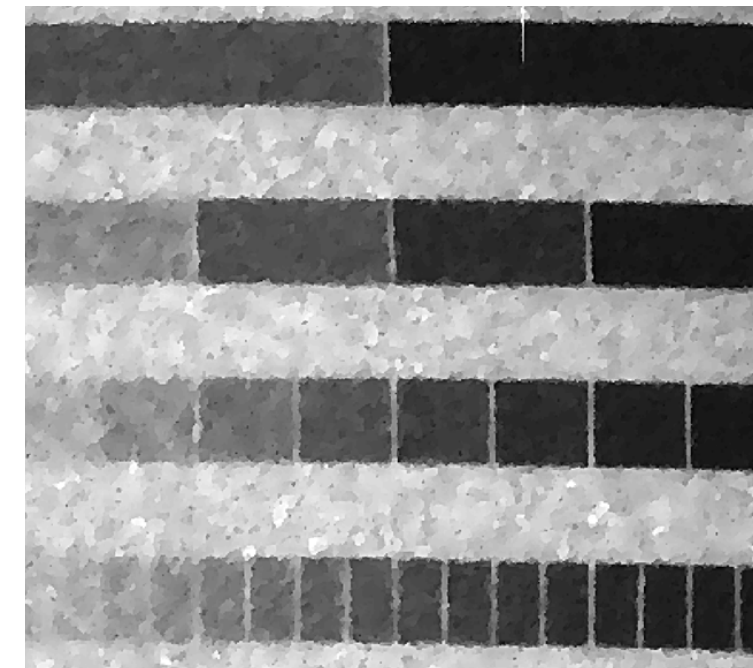
# Results: Reflectivity chart



Reference measurement  
(~1000 photos/pixel)

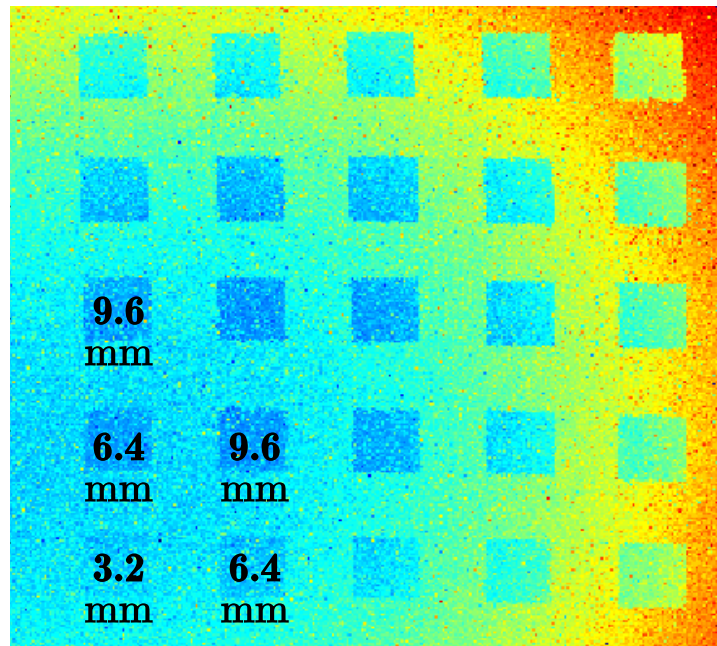


First-photon ML estimate

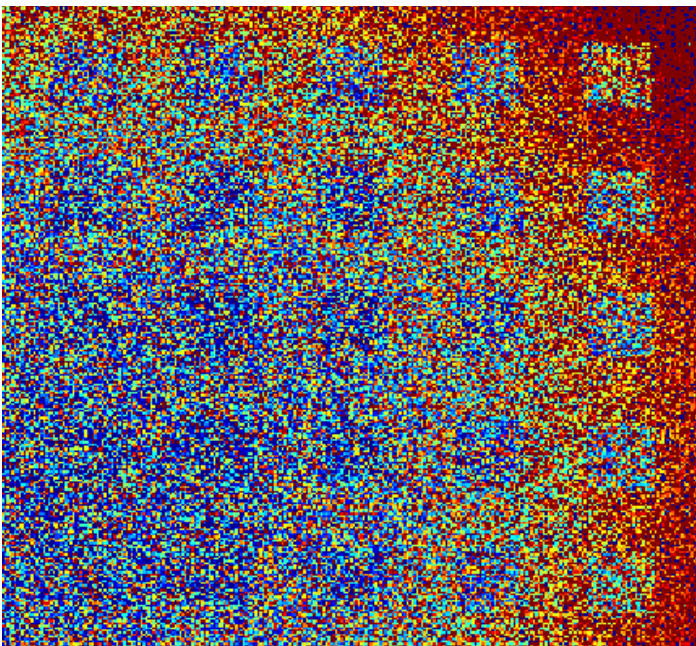


First-photon, reconstructed

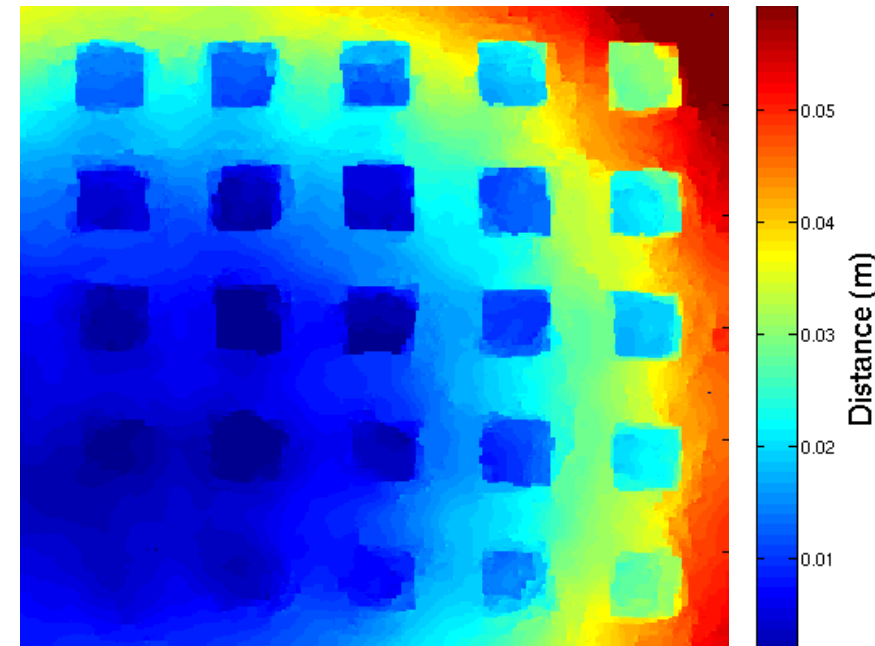
# Results: Depth chart



Reference measurement  
(~1000 photos/pixel)



First-photon ML estimate



First-photon, reconstructed



# SPAD array imaging

Established research collaboration with  
Zappa group, Politecnico di Milano

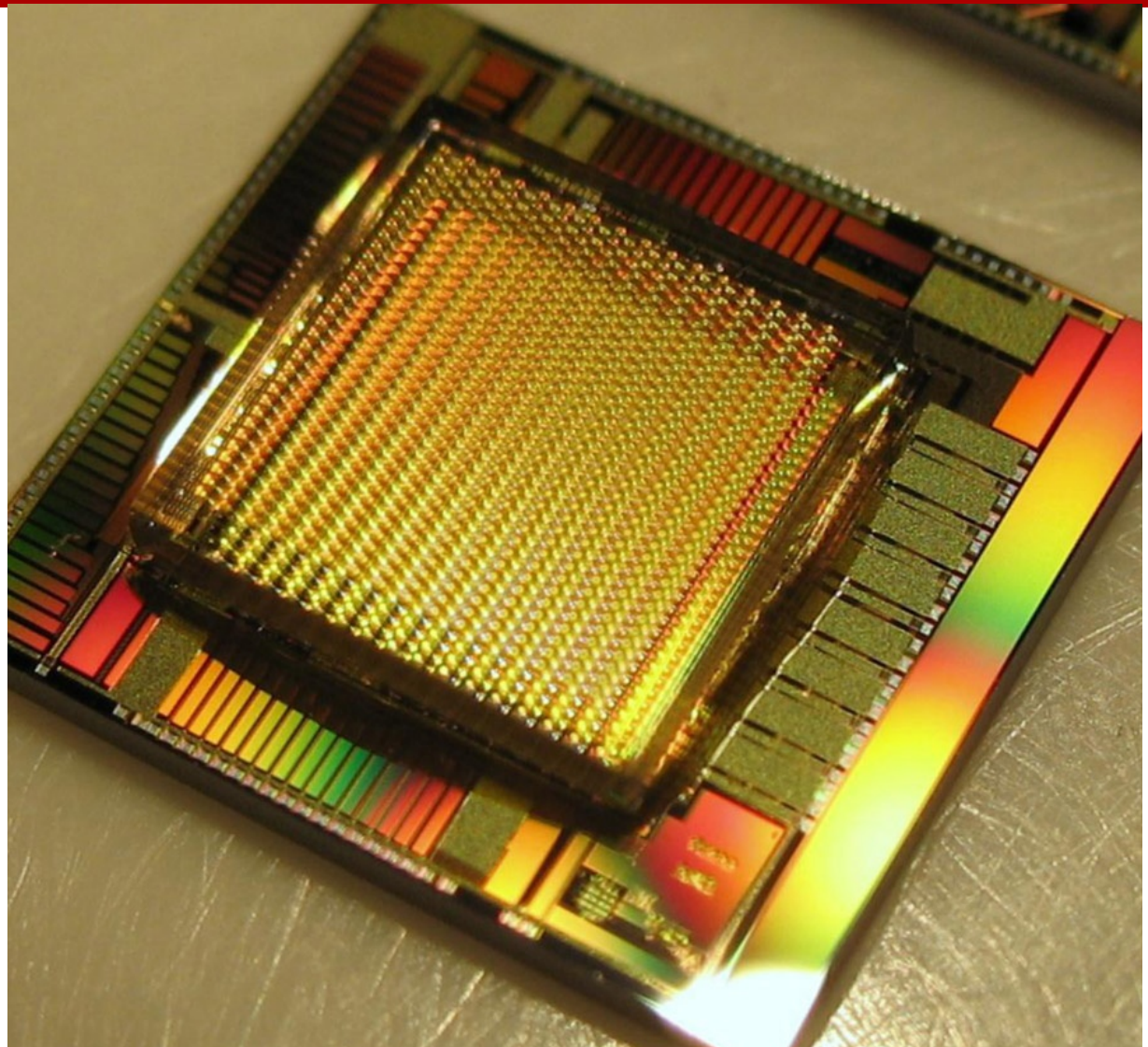
Borrowed prototype of a 32×32 pixel  
SPAD array with 6-bit TDC at each pixel

## **Counting mode:**

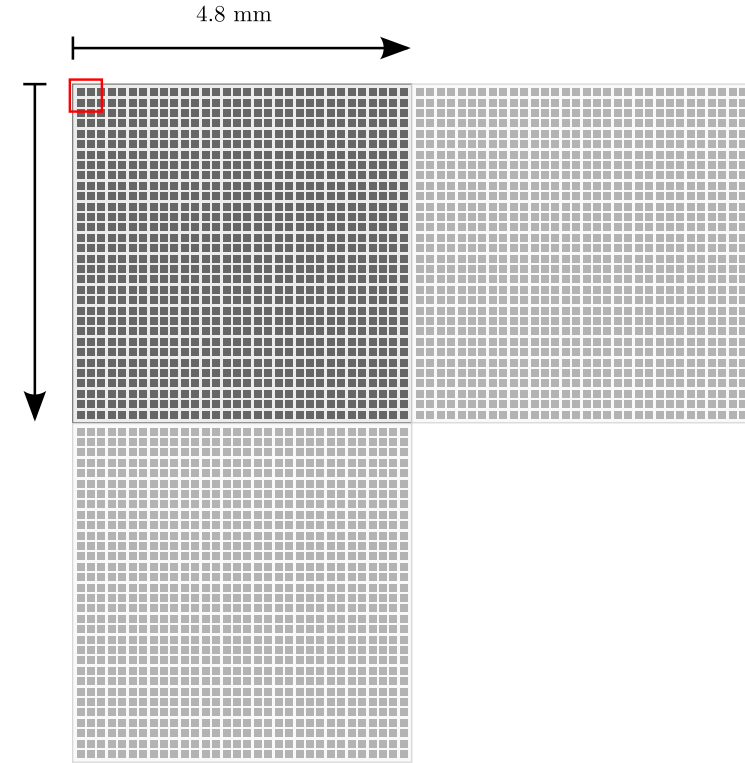
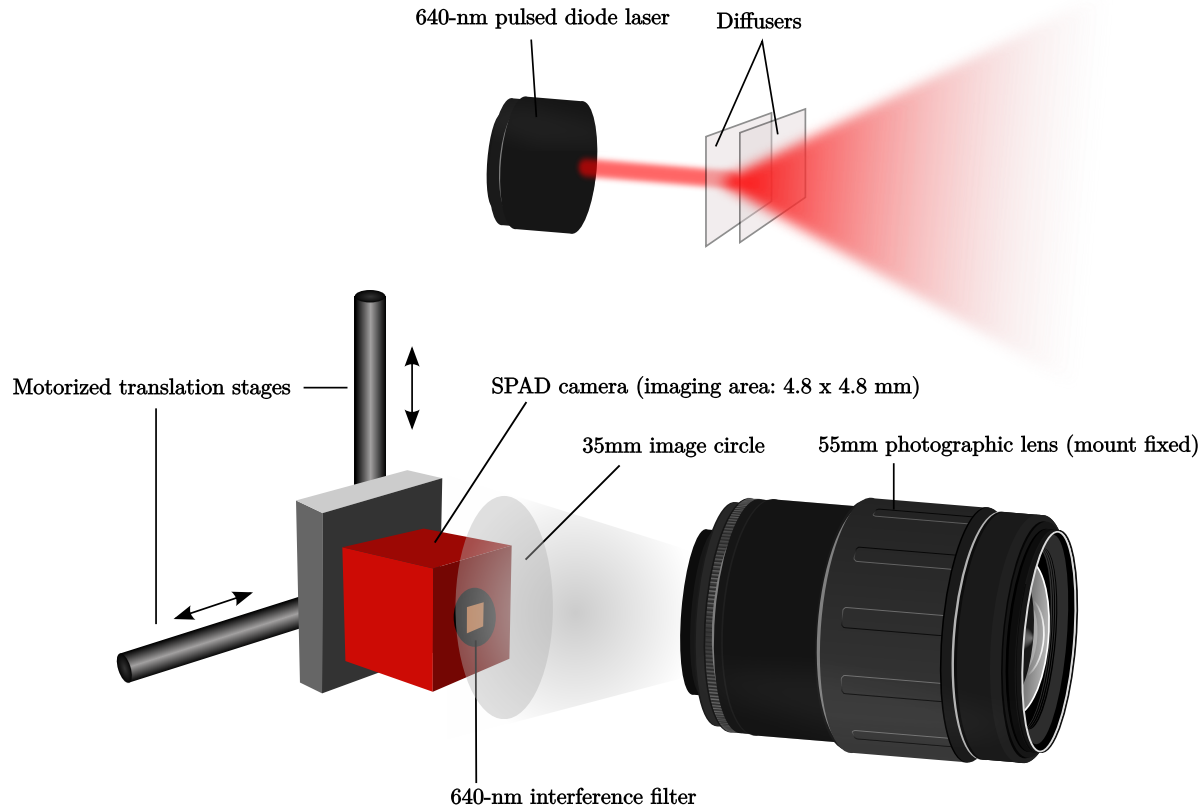
6-bit resolution (0-63 photon arrivals)

## **Timing mode:**

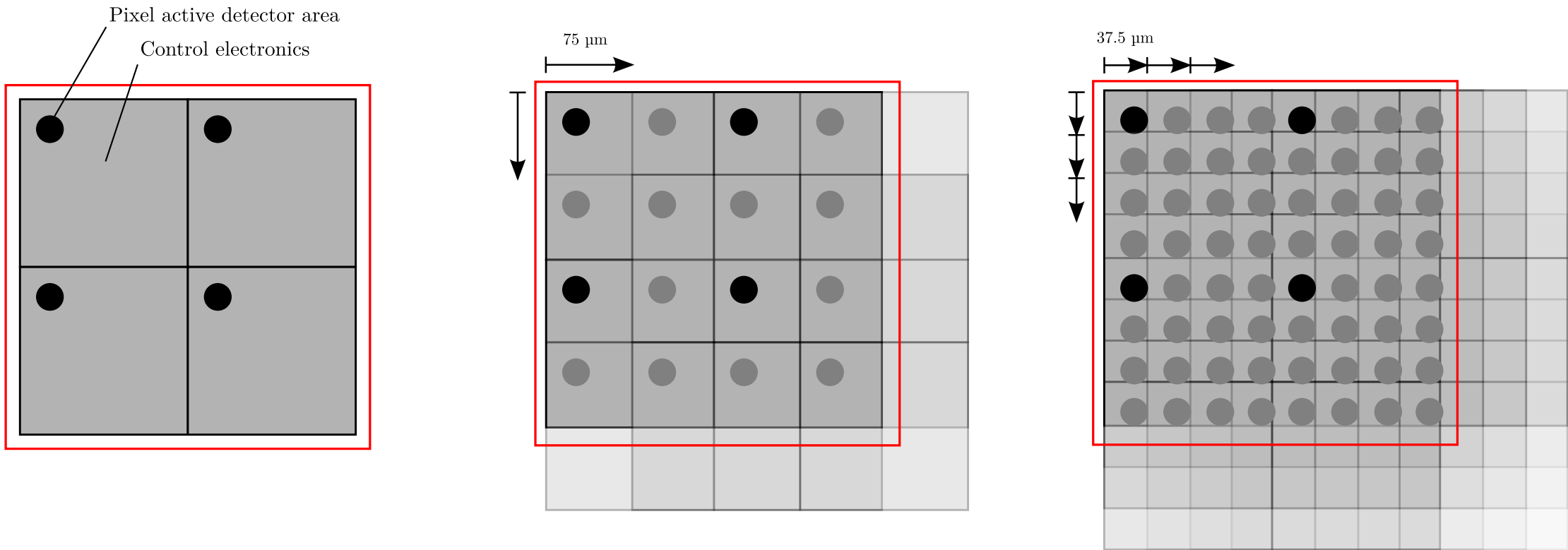
10-bit, 1024 bins, each 389.9 ps



# SPAD array imaging



# Subpixel scanning for higher resolution



# Computational reconstruction algorithm

## Step 1: Reflectivity reconstruction

Instead of time until first arrival, we now use the number of photon detection events in a fixed dwell period.

$$\mathcal{L}(\alpha(x, y) | n(x, y)) = \gamma [\alpha(x, y)S + BT_r] [n(x, y) - 1] - \log [\gamma\alpha(x, y)S + BT_r]$$



$$\mathcal{L}(\alpha(x, y) | k(x, y)) = \gamma [\alpha(x, y)S + BT_r] [N - k(x, y)] - k(x, y) \log [1 - \exp [-\gamma\alpha(x, y)S + BT_r]]$$

# Computational reconstruction algorithm

## Step 2: Background noise censoring

1. Compute  $t_{ROM}(x, y)$  = median value of all detections in neighboring 8 pixels
2. Define a set of indices of detections to keep as valid, rejecting the others.

$$U(x, y) = \left\{ \ell : |t_\ell(x, y) - t_{ROM}(x, y)| < 2T_p \left( \frac{BT_r}{\gamma\alpha(x, y)S + BT_r} \right), 0 \leq \ell < k(x, y) \right\}$$

# Computational reconstruction algorithm

## Step 3: Depth reconstruction

Instead of using only first arrival, we make use of all valid data.

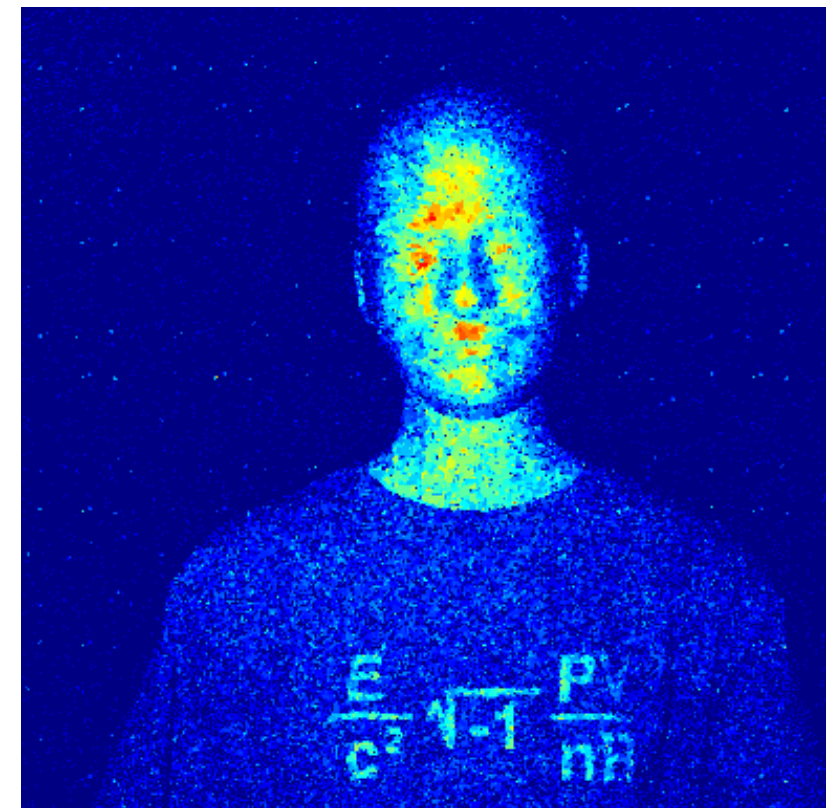
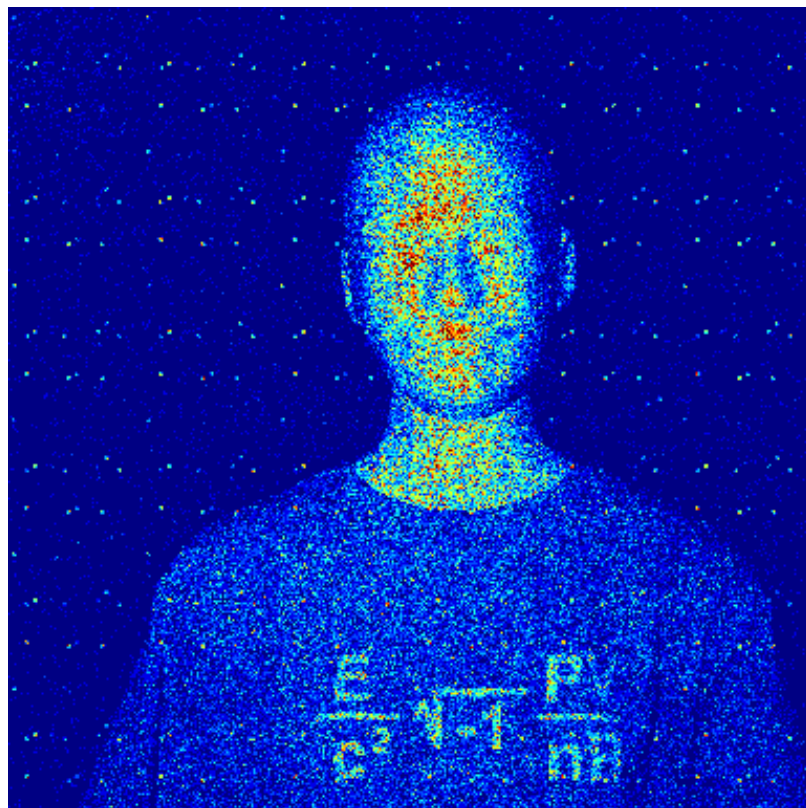
$$\mathcal{L}(Z(x,y)|t(x,y)) = -\log \left[ s(t(x,y) - \frac{2Z(x,y)}{c}) \right]$$



$$\mathcal{L}(Z(x,y)|\{t_\ell(x,y)|\ell \in U(x,y)\}) = -\sum_{\ell \in U(x,y)} \log \left[ s(t_\ell(x,y) - \frac{2Z(x,y)}{c}) \right]$$

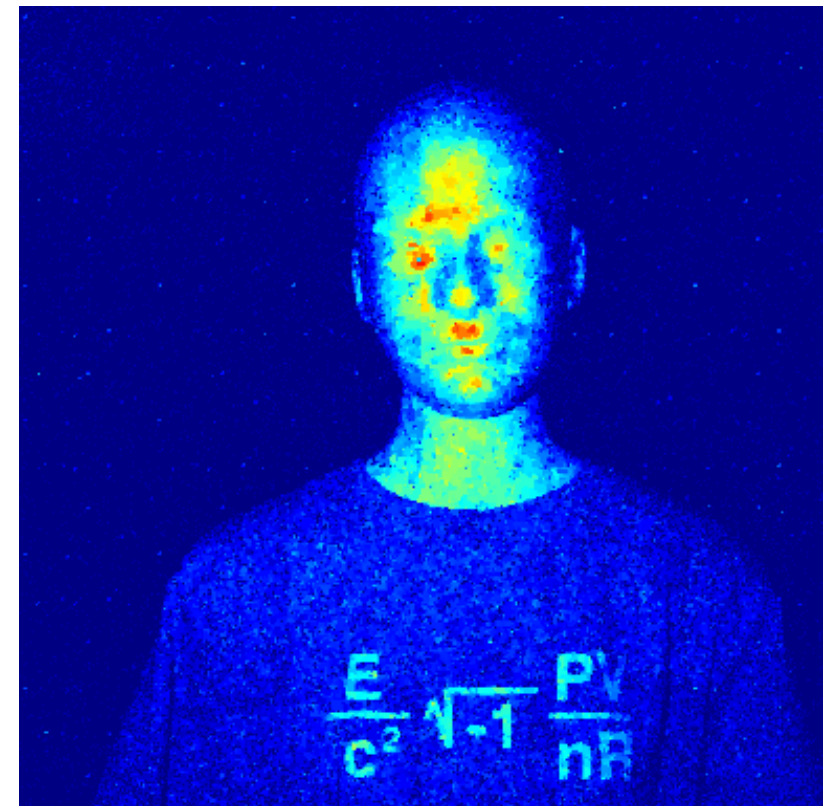
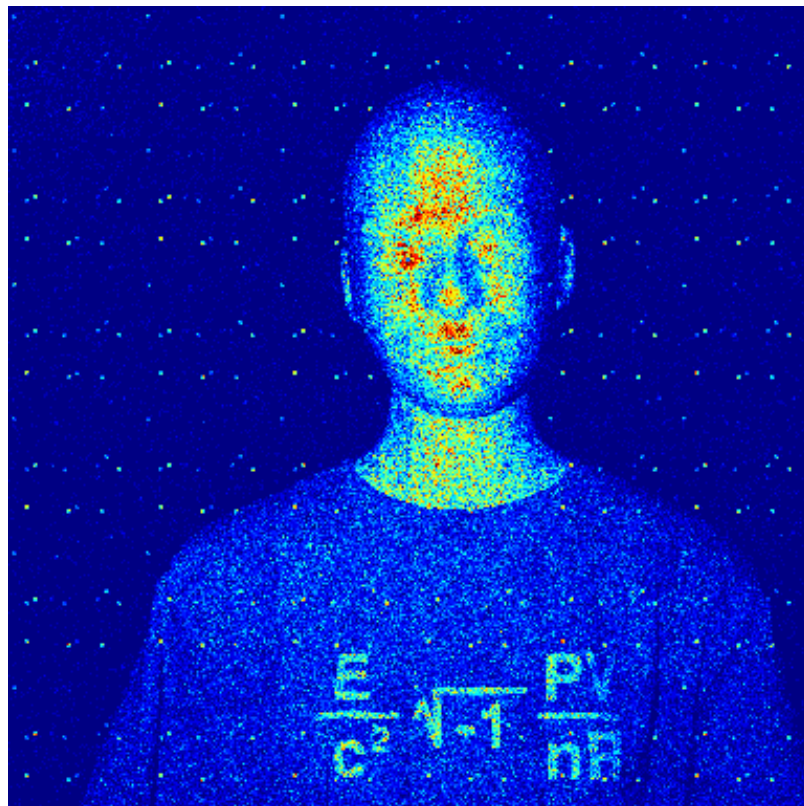
# Preliminary results: Reflectivity

25 frames



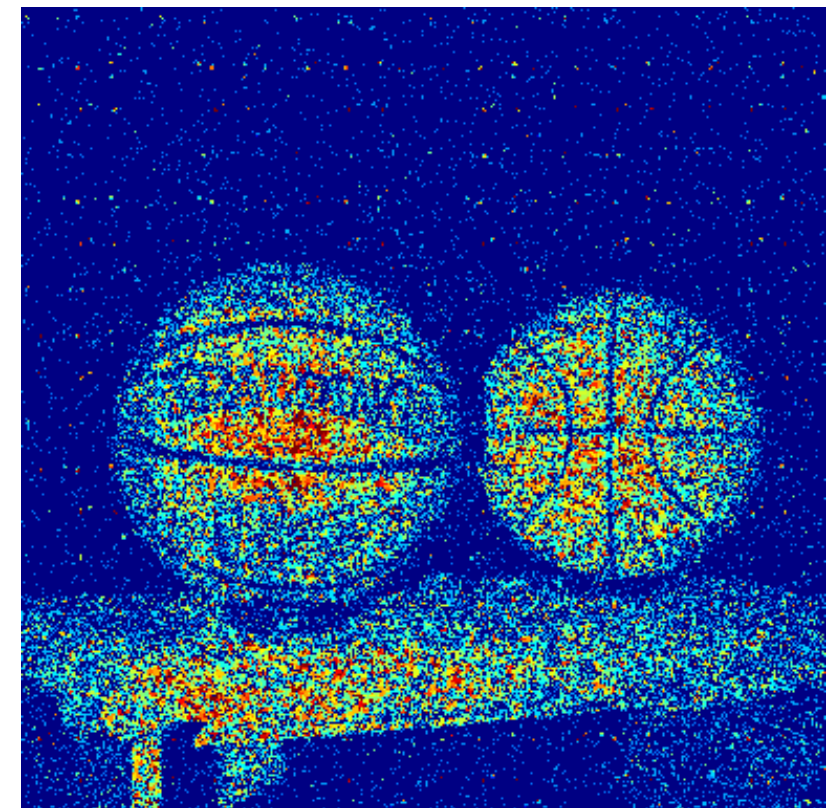
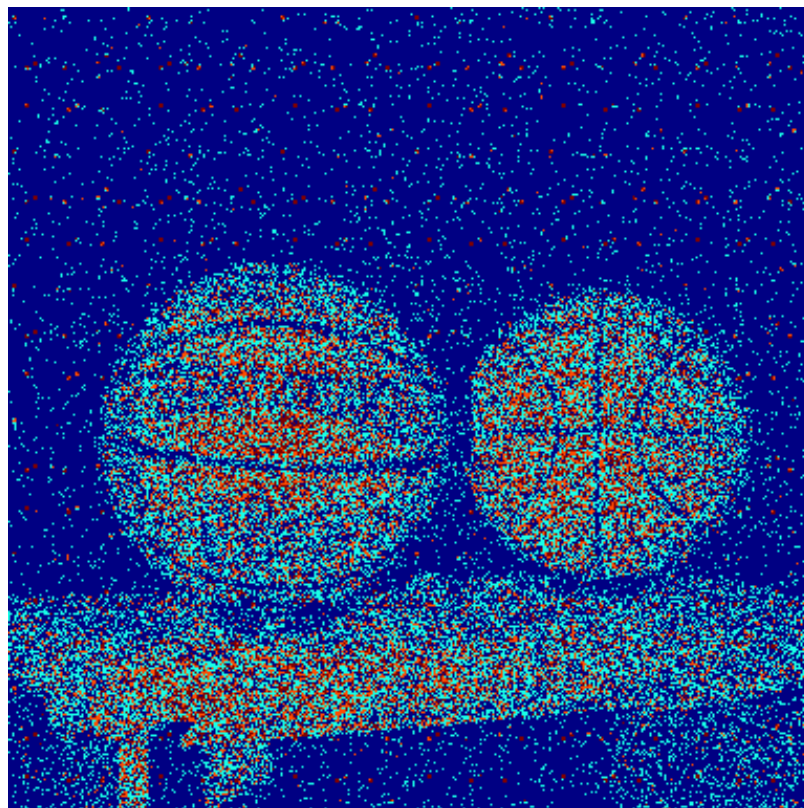
# Preliminary results: Reflectivity

50 frames



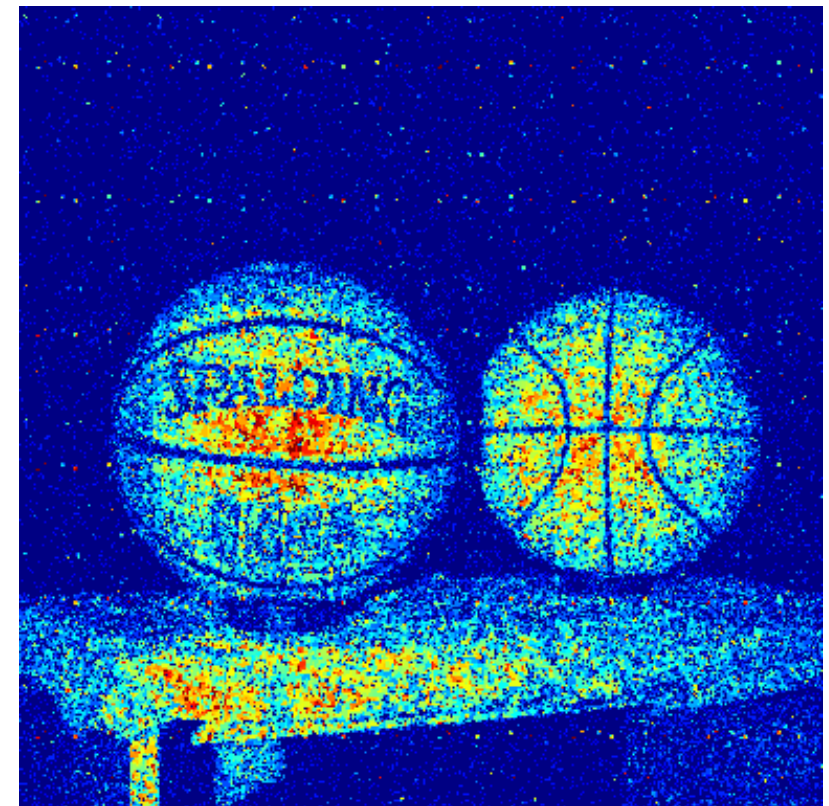
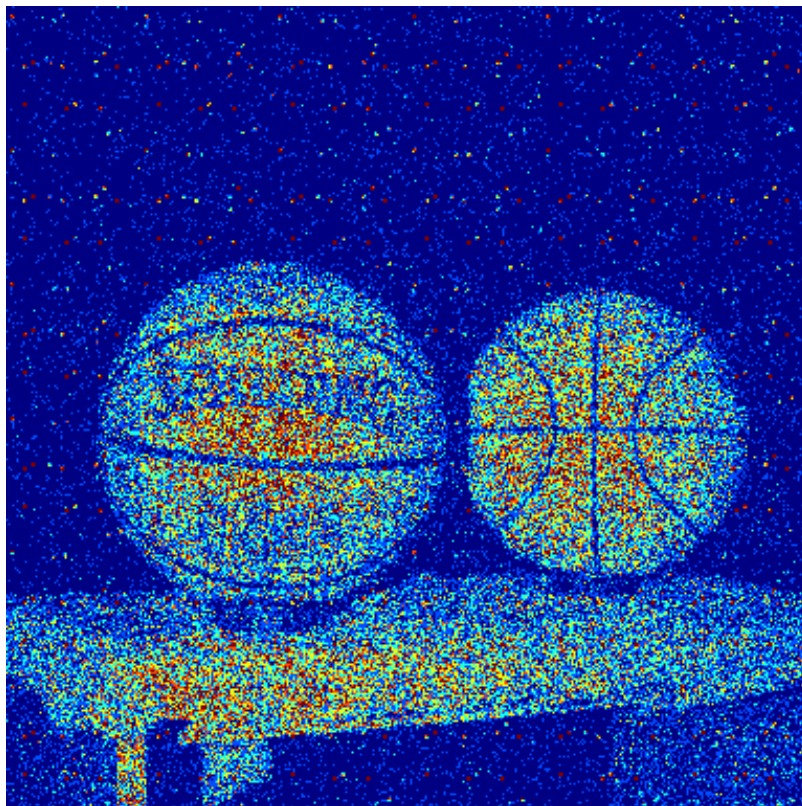
# Preliminary results: Reflectivity

25 frames



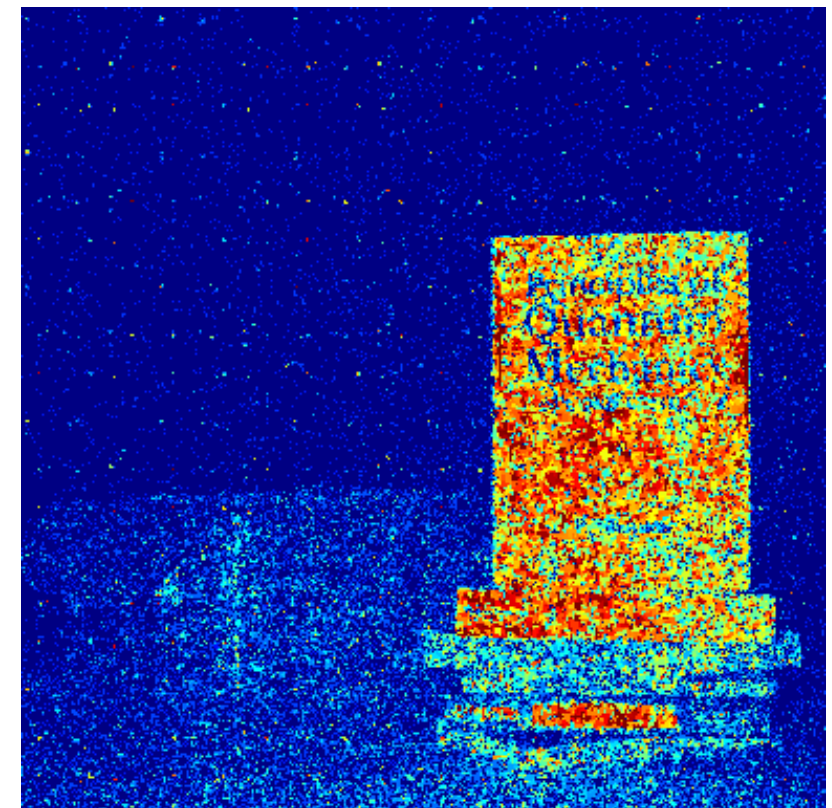
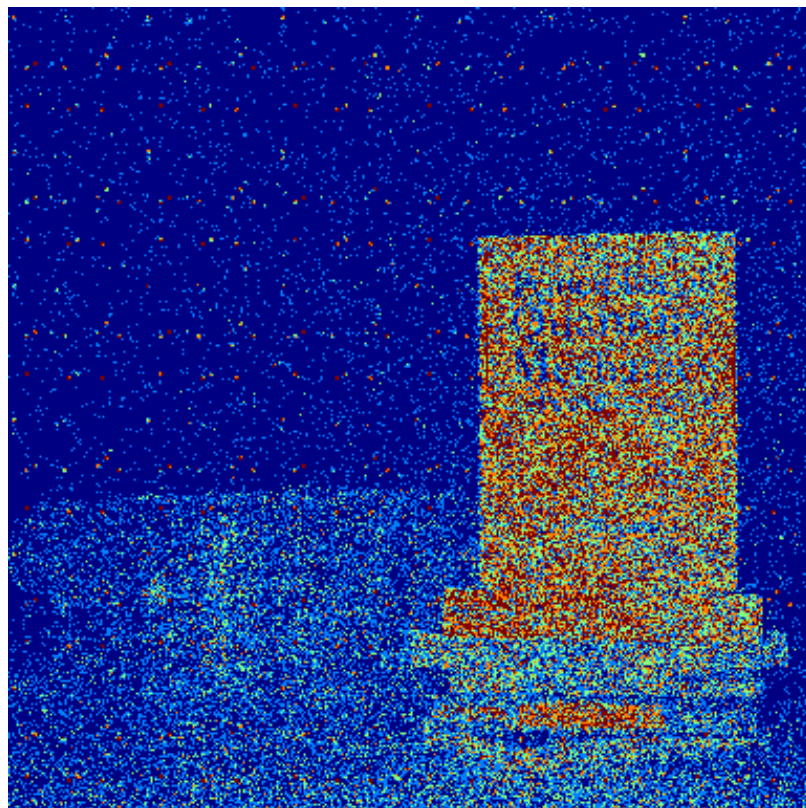
# Preliminary results: Reflectivity

50 frames



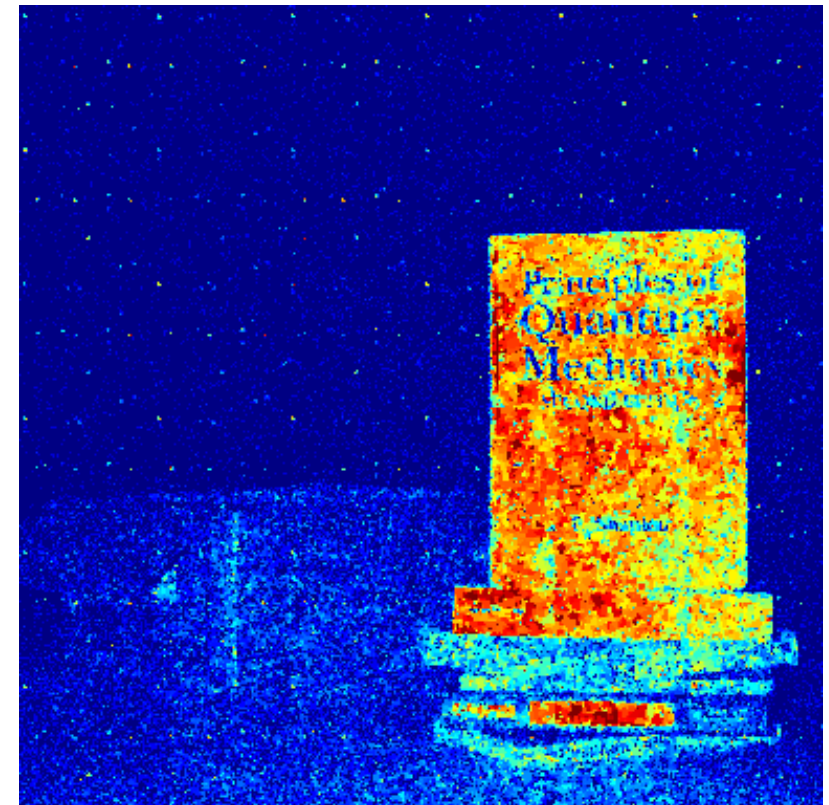
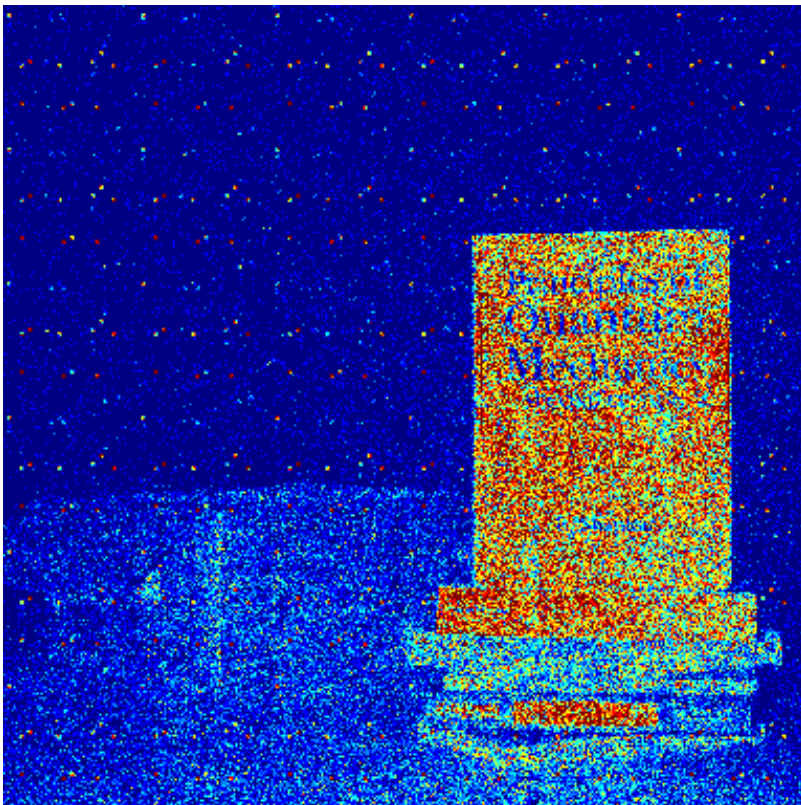
# Preliminary results: Reflectivity

25 frames



# Preliminary results: Reflectivity

50 frames



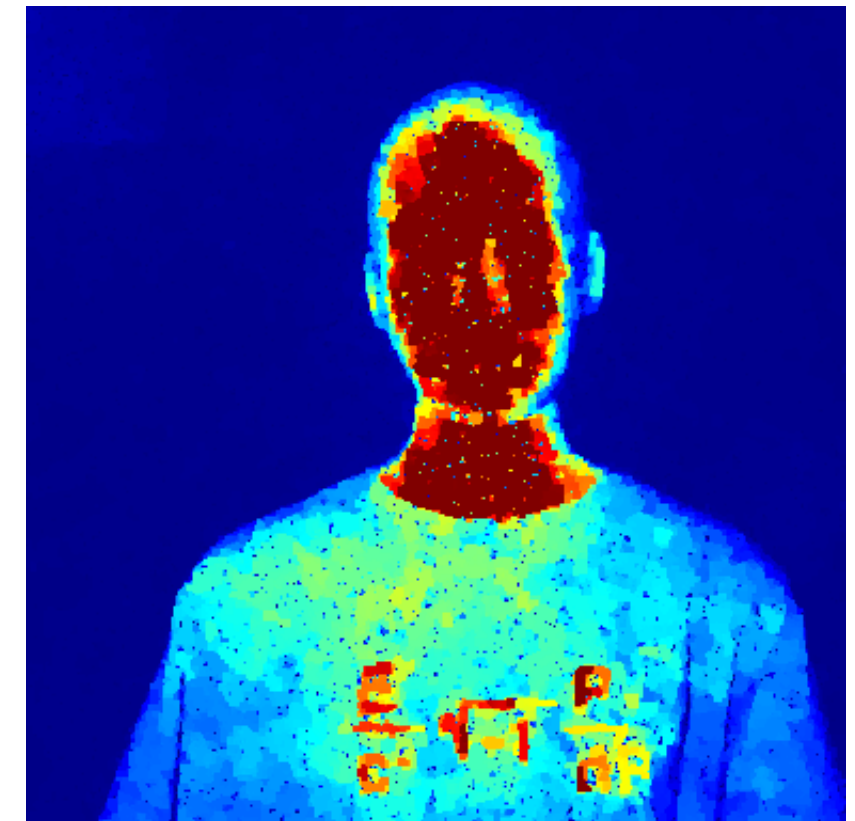
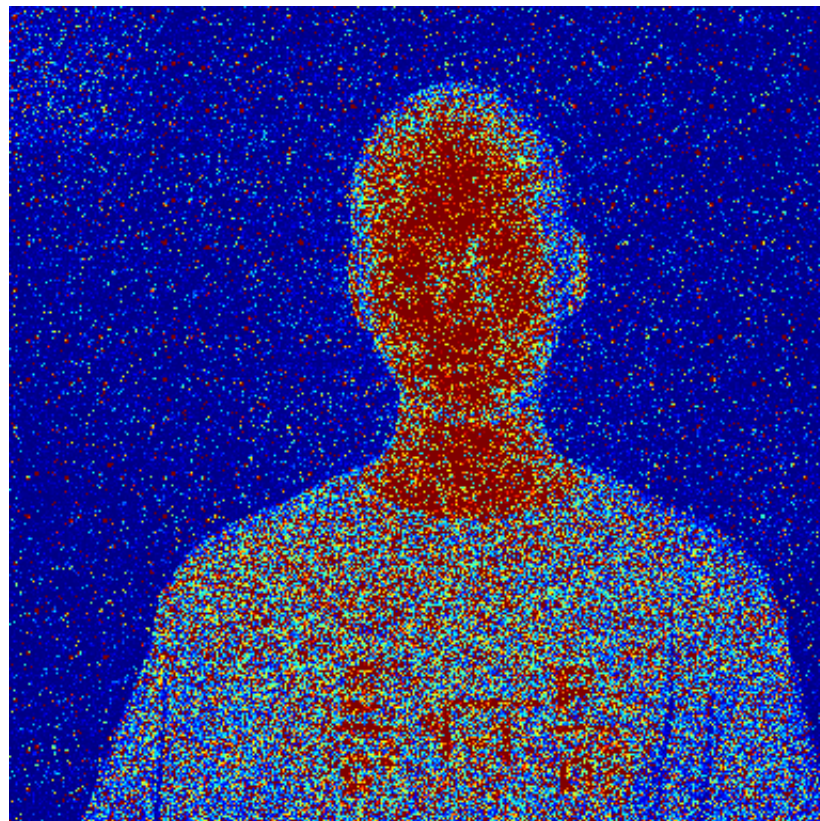
# Preliminary results: Reflectivity

## **Results not as striking as first-photon imaging**

- » Fixed-dwell time severely impacts dynamic range
- » Many pixels with no detection events
- » Need global long dwell times to get any detections in dark regions
- » Traditional averaging begins to work well for longer dwell times

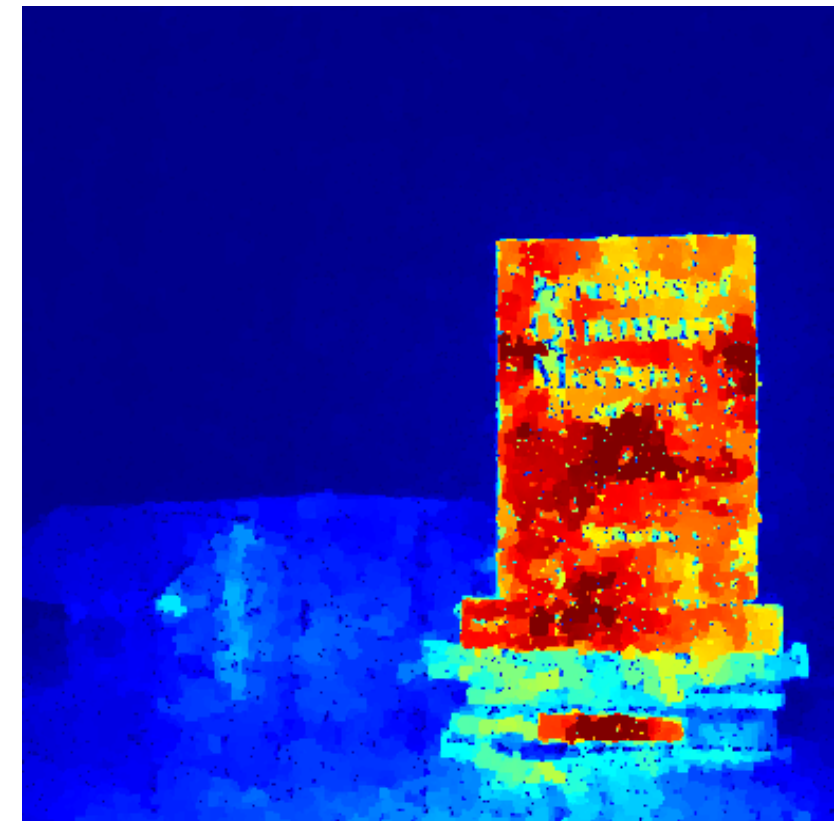
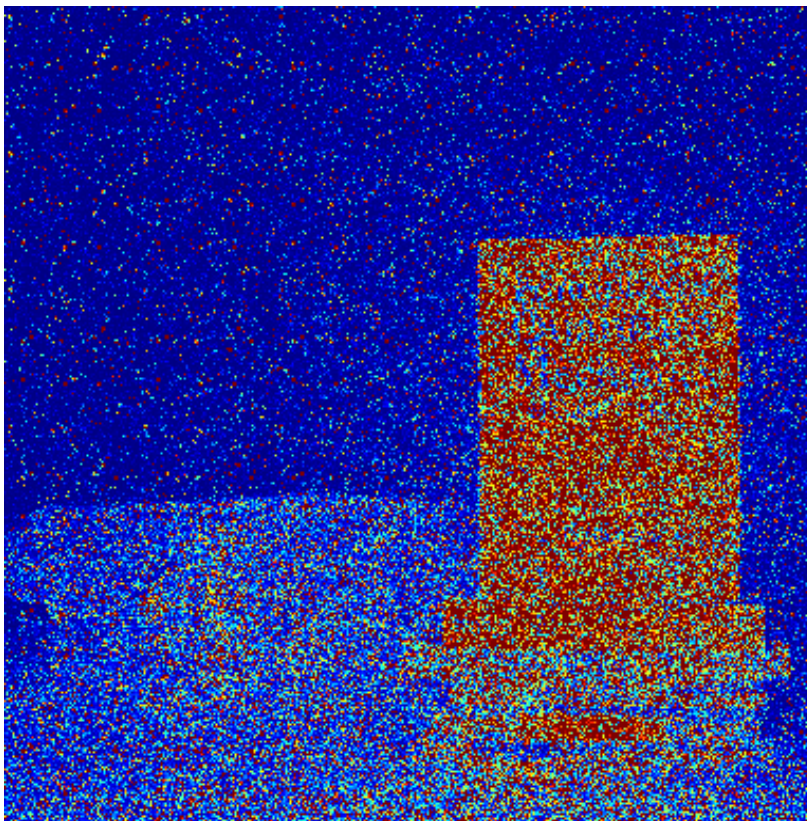
# Preliminary results: Reflectivity

Simulated FPI



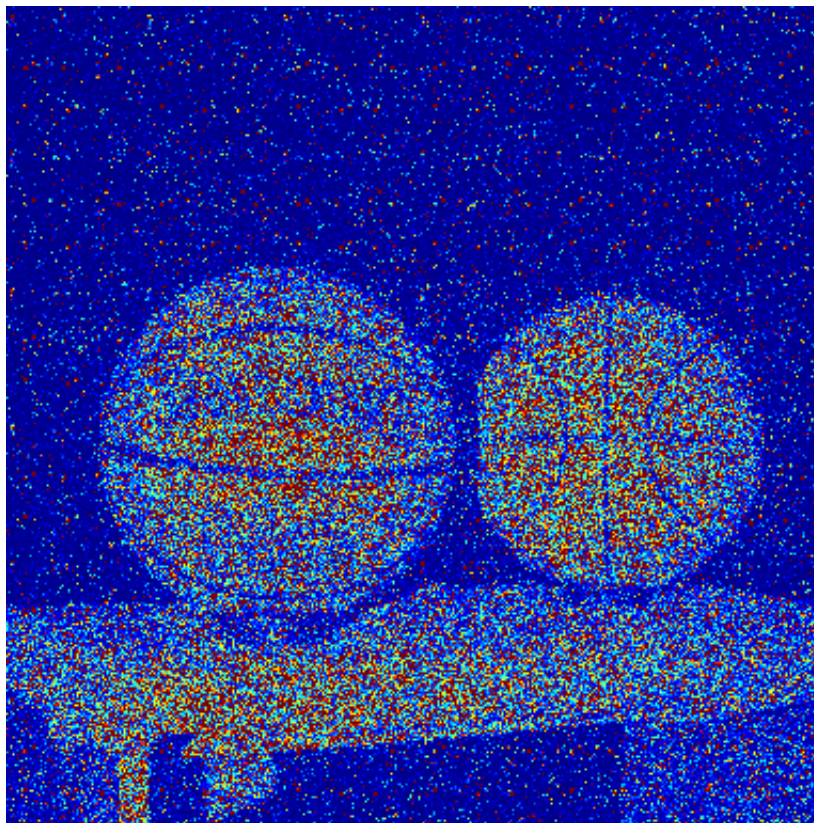
# Preliminary results: Reflectivity

Simulated FPI



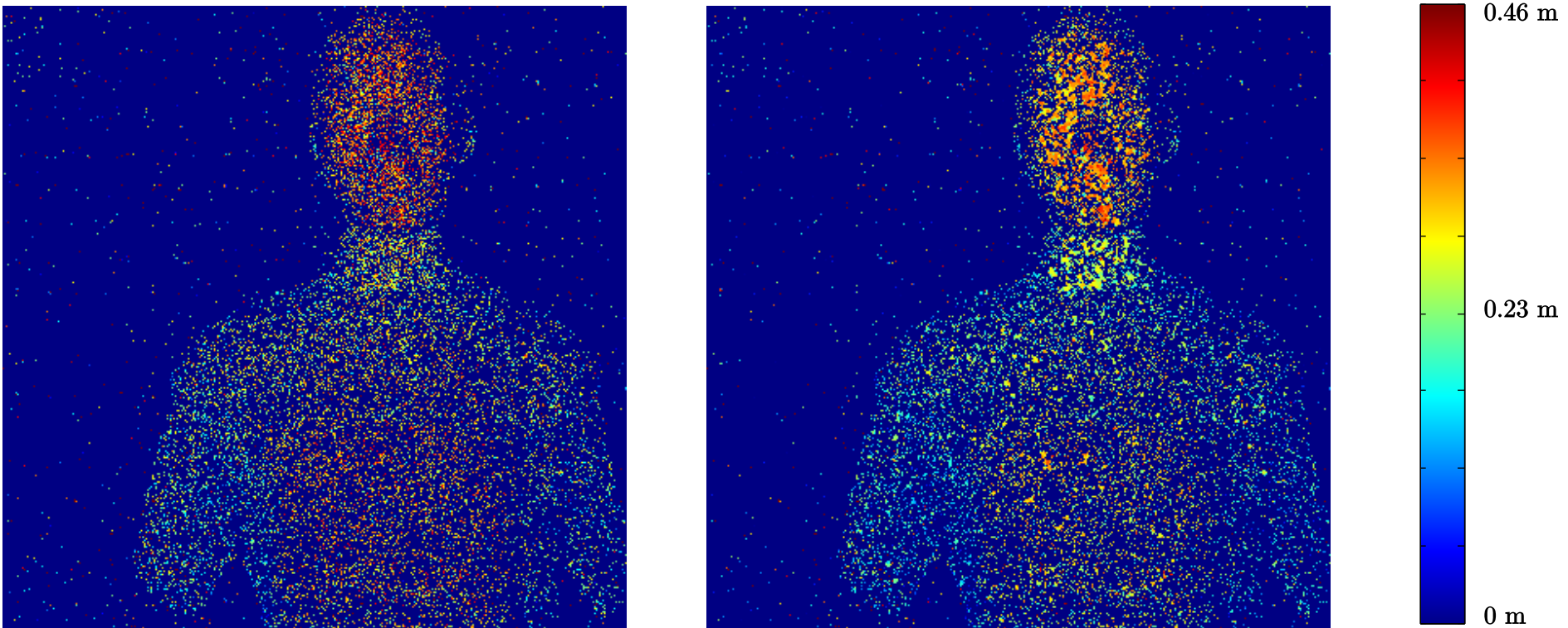
# Preliminary results: Reflectivity

Simulated FPI



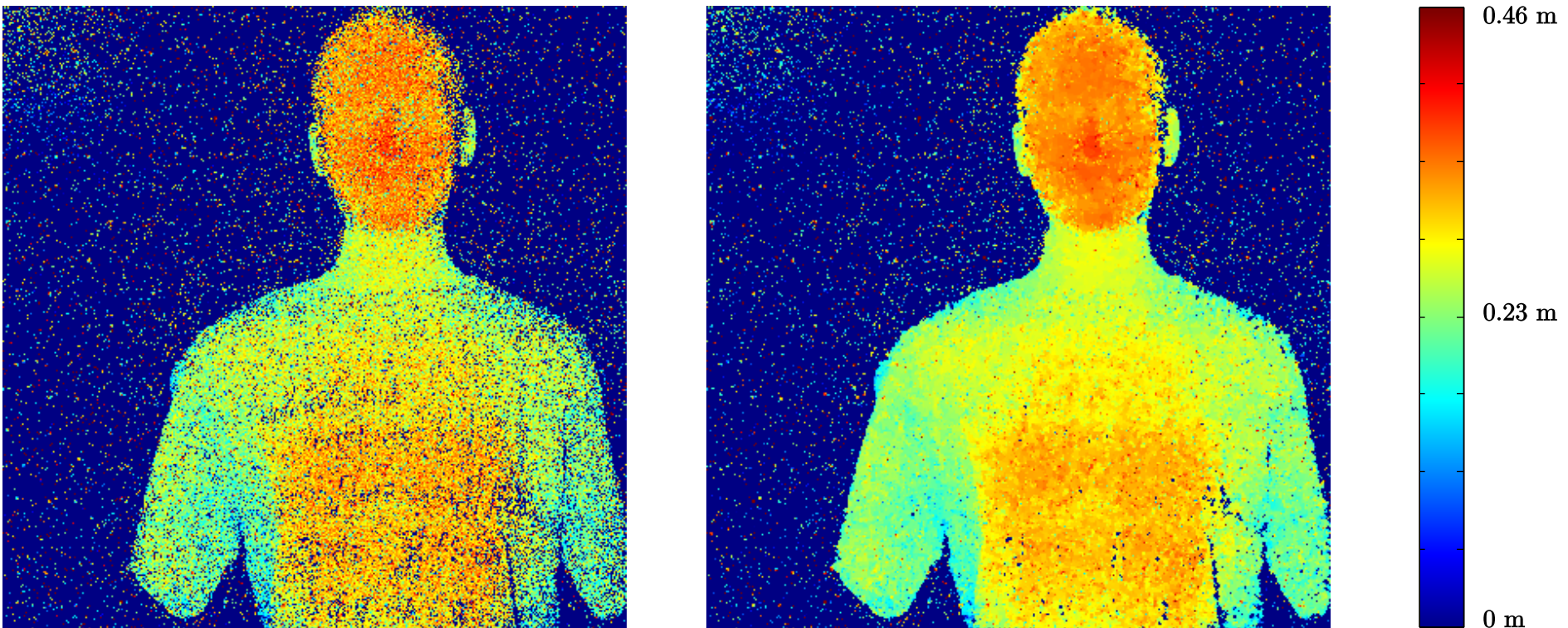
# Preliminary results: Depth

25 frames



# Preliminary results: Depth

400 frames



# Preliminary results: Depth

## **Mismatch of laser pulse, object features, and time bin size**

- » FPI: time bin (8 ps) < features (~50 ps) < pulse width (226 ps)
- » SPAD: time bin (389.9 ps) > pulse width (226 ps) > features (~50 ps)

## **Future experiments:**

- » Change illumination to 1-2 ns pulse width
- » Change object to large, several-meter sized objects
- » SPAD arrays with improved time resolution

# 5 CONCLUSIONS

# PC-OCT conclusions

## **Built classical phase-sensitive source**

- » Amplified SPDC in entanglement-breaking regime

## **Implemented PC-OCT**

- » Factor-of-2 resolution improvement as seen in Q-OCT
- » Even-order dispersion cancellation as seen in Q-OCT
- » Much faster acquisition possible with classical illumination/detection

# GI conclusions

## **Built a second classical phase-sensitive source**

- » Using 50/50 beamsplitter and a pair of SLMs
- » Computer-driven with deterministic, pseudorandom phase patterns
- » Capable of both phase-insensitive and phase-sensitive operation

## **Implemented phase-sensitive classical far-field GI**

- » Inverted image as seen in biphoton-based GI
- » High-speed acquisition with classical illumination and detection

# GI conclusions

## **Implemented computational GI**

- » Reference arm replaced with computational simulation

## **Implemented compressive GI**

- » Factor-of-10 speedup by assuming object is spatially sparse

## **Explored computational + compressive GI**

- » Need SLM with more predictable operation

# Single-photon imaging conclusions

## First-photon imaging

- » Established collaboration with STIR group at MIT
- » Used techniques similar to compressed sensing to acquire high-quality depth and reflectivity images using 1 photon per pixel
- » Factor-of-100 speedup from traditional active imagers
- » Factor-of-10 sub-pulse depth resolution
- » 3-4 bit intensity resolution

# Single-photon imaging conclusions

## SPAD array imaging

- » Established collaboration with Zappa group at PdM
- » Adapted FPI algorithm to fixed dwell time case
- » Acquired and processed initial set of data
- » Reflectivity shows improvements but dynamic range limited
- » Depth images need larger objects and/or a longer pulse to show improvements using algorithm

# Acknowledgements

## **Advisors / Thesis committee**

Franco N. C. Wong, Jeffrey H. Shapiro, Vivek K. Goyal

## **Collaborators**

Ahmed Kirmani, Andrea Colaço, Dongeek Shin, Rudi Lussana, Franco Zappa, Julien Le Gouët

## **Group members**

Zheshen Zhang, Sara Mouradian, Murphy Niu, Valentina Schettini, Maria Tengner, Raúl García-Patrón, Veronika Stelmakh, Tian Zhong, Taehyun Kim, Onur Kuzucu, Saikat Guha, Nicholas Hardy, Baris Erkmen